2011

Evaluation and Prediction of Microstructure Evolution in Deformed Aluminum Alloys

Nabeel Hussain Alharthi
Lehigh University

Evaluation and Prediction of Microstructure Evolution in Deformed Aluminum Alloys

by

Nabeel Hussain Alharthi

A Thesis

Presented to the Graduate and Research Committee

of Lehigh University

in Candidacy for the Degree of

Master of Science

in

Mechanical Engineering and Mechanics

Lehigh University

Bethlehem, PA

May, 2011

This thesis is accepted and approved in partial fulfillment of the requirements for the Master of Science.

_____

Date

_____

Thesis Advisor: Prof. Wojciech Z. Misiolek

_____

Chairperson of Department: Prof. D. Gary Harlow

ACKNOWLEDGMENTS

Foremost, I would like to thank ALLAH for helping me in my life and for giving me the ability to continue this work. Then, I would like to give my most respect and loving to my great parents who support me since I was a child. I dedicate this work to them. Also, I would thank my lovely wife and my children for their patient and continuous support. Many thanks to my family.

I would also like to thank my advisor Prof. Wojciech Z. Misiolek for his technical guidance and encouragement throughout my master degree at Lehigh University.

Special thanks for my best friend Bandar Alzahrani for his support, technical discussions, sharing ideas. He is like my brother since we went through undergraduate studies together.

I would like to thank my colleagues in Institute for Metal Forming at Lehigh University for useful discussion. Also, I would like to thank Prof. Antoinette M. Maniatty from Rensselaer Polytechnic Institute for providing the samples of the asymmetrical rolling project. Also, many thanks to Sam Lawrence and William Mushock for their guidance in the lab.

Finally, I would like to thank King Saud University for supporting me financially to pursue my Master of Science degree from Lehigh University.

Table of Contents

LIST OF FIGURES

LIST OF TABELS

ABSTRACT

The understanding of the microstructure evolution during the deformation processes is very important to predict the mechanical properties of the deformed workpiece. In the present work two aluminum alloys from different series were studied in two different deformation processes.

The first part is the surface grain structure evolution in AA6082 hot direct extruded shapes with different ram speeds (0.25, 0.5, 1, 2 mm/sec). The samples were characterized by the light optical microscopy (LOM) and by electron backscatter diffraction (EBSD) to measure the grain size and misorientation angle in the thickest part of the extrudates. Also, numerical simulation process was performed by a finite element package DEFORM™ −3D to obtain the state variables such as stress, strain, strain rate, temperature and their distribution in the deformation zone. These state variables were incorporated in a joint dynamic recrystallization model which is developed by Bandar and modified by Depari and Misiolek to predict the surface grain structure and the misorientation angle . The experimental results showed a good agreement with the model predictions.

The second part is focused on the microstructure evolution of asymmetrically rolled AA-5182. Asymmetric Rolling (ASR), where the linear speeds at the surfaces of the upper and lower roll differ in order to impose shear within the workpiece, has been shown to be a promising, economical approach to altering the microstructure of rolled aluminum alloy sheet. The purpose of this process is to produce intense shear deformation throughout the entire sheet thickness, as opposed to superficial shear

deformation imposed by conventional rolling. The microstructure response to the ASR process conditions for the aluminum alloy AA5182-O was analyzed using metallographic techniques. The initial sample microstructure and the deformed microstructure after the first and fourth passes were analyzed at three locations in each sample - near the top surface where contact with the upper roll took place, near the mid-plane, and near the bottom surface where contact with the lower roll took place. In each case, the microstructure was examined in the rolling direction (RD) and the normal direction (ND). The results show that the grain size varies within the samples and even more between the samples representing different stages of the ASR process. However, for the reported rolling conditions, the fine grain structure has not been produced.

1 CHAPTER 1: INTRODUCTION

1.1 *Aluminum and its Alloys*

Aluminum is one of most used metallic element on earth[1].It is used in many engineering applications such as automotive, constructions, buildings, packaging… etc. Also, It also is involved in a lot of modern life applications and has more than three hundred alloys ranging from pure Aluminum to complex alloys with different physical and mechanical properties. Therefore, Aluminum is attractive and common in industry because of its appearance, light weight, formability, and corrosion resistance.

One of the most important properties of Aluminum is its density of 2.7 g/cm^3, approximately one third of the value for steel (7.83 g/cm^3), Copper (8.93 g/cm^3), or Brass (8.53 g/cm^3). Moreover, Alumium is a reflective and has high thermal conductivity, about 50 to 60% that of copper and it is nontoxic.

Aluminum and its alloys may be cast or processed in wrought form by many manufacturing processes such as rolling, extrusion, forging, stamping, powder metallurgy to form sheet, plate, foil, rod, bar, wire, tube, pipe, structural forms and metal-matrix composites. The final stage of Aluminum products can also be achieved in one of the machining processes.

Among the most important characteristic of Aluminum is its high formability. The strength, ductility give a good combination of forming flexibility. In addition, the heat-treatable Aluminum alloys can be formed which result in a high strength to weight ratio.

Aluminum alloys can be divided into two major categories: casting compositions and wrought compositions. Additionally, wrought alloys can be classified as heat

treatable (HT) and non heat treatable . For wrought alloys a four-digit system is used to produce a list of wrought composition families as follows[1]:

- 1*xxx* Controlled unalloyed (pure) compositions.
- 2*xxx* Alloys in which Copper is the principal alloying element, though other elements, notably Magnesium, may be specified.
- 3*xxx* Alloys in which Manganese is the principal alloying element.
- 4*xxx* Alloys in which Silicon is the principal alloying element.
- 5*xxx* Alloys in which Magnesium is the principal alloying element.
- 6*xxx* Alloys in which Magnesium and Silicon are principal alloying elements.
- 7*xxx* Alloys in which Zinc is the principal alloying element, but other elements such as Copper, Magnesium, Chromium, and Zirconium may be specified.
- 8*xxx* Alloys including Tin and some Lithium compositions characterizing miscellaneous compositions.
- 9*xxx* Reserved for future use.

In the present work, I have focused on two aluminum alloys which are AA 5182 and AA 6082. The 5*xxx* series has Magnesium as the major alloying elements where Magnesium is an effective element to increase the hardness of the alloy and when the Manganese is added to Aluminum, the result is a good work-harden alloy. Also, alloys in this series have good welding characteristics and good resistance to corrosion. This series is used in beverage cans and can ends; home appliances; and automotive industry[2].

6*xxx* series contains Silicon and Magnesium which form Mg_2Si. It allows the alloy to be heat treatable. In addition this series has a medium strength, good formability, machinability, weldability, and corrosion resistance when compared to 2xxx and 7xxx

series. Uses include transportation equipment, architectural applications, bridge railings, and welded structures.

Table 1. AA 5182 and AA 6082 chemical compositions, weight %

Alloy	Si %	Fe %	Cu %	Mn %	Mg %	Cr %	Zn %	Al %
5182	0.20	0.35	0.15	0.20-0.50	4.0-5.0	0.10	0.25	BAL
6082	0.7-1.3	0.50	0.10	0.40-0.10	0.6-1.2	0.25	0.20	BAL

1.2 *Types of Aluminum Products*

Formed aluminum products are classified to five major categories based on deformation processes and geometry of the final product , the following categories are:

- Flat-rolled products (sheet, plate, and foil)
- Rod, bar, and wire
- Tubular products
- Shapes
- Forgings

The term mill product is used for the extruded rod, bar, wire tubular products, and shapes. However Aluminum forgings are not considered mill products.

1.3 *Forming of Aluminum Alloys*

Aluminum and its alloys are considered to be one of the most formable metals and alloys. Materials formability depends on the amount of alloying elements see Fig.1 [3]. Moreover, general material formability cannot be restricted only to the yield strength or work hardening, ductility, strain rate but also it should include the ease of machining and consistency of the finished products in mass production according to Kazanowski [3].

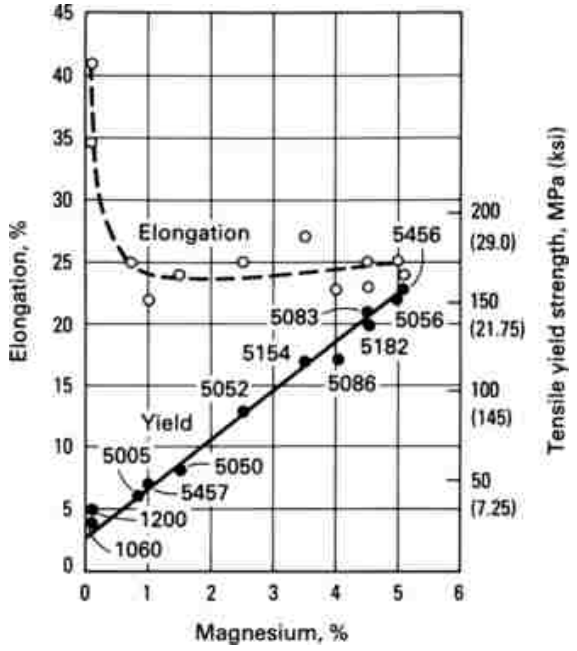

Figure 1. Correlation between tensile yield strength, elongation, and magnesium content for some commercial aluminum alloys in the annealed temper[3]

On the other hand deformation failures of aluminum alloys such as cracking or splitting can be caused by ductile fracture. It can start from the crack nucleation points and connect them to microscopic voids and/or by localized strain at the shear bands the fracture could appear. In the following sections two forming processes namely extrusion and rolling will be discussed since they were the subject of performed materials investigations.

1.4 *Extrusion*

Extrusion is a process in which wrought products are formed by forcing a heated billet through a die opening with a required shape[4]. There are many classifications of extrusion process based on temperature, lubrication and relative motion between the ram and the billet.

In terms of temperature, there is hot extrusion where the process is performed at elevated temperature above recrystalization temperature which is about 60% of the material melting temperature. In contrast, the cold extrusion is performed at room temperature or close to it. Finally, warm extrusion is performed above the room temperature and below the recrystalization temperature. Some materials cannot be formed by the cold extrusion especially when the shape is too complex. On the other hand, hot extrusion is used to produce different shapes such as rods, bars, tubes, strips and wires.

The second classification is based on the lubrication. As a consequence of that, there are three different types[5].

1) Nonlubricated extrusion process where a flat-face die is used and the billet is pushed inside the container where the dead metal zones are formed between the container and the die as shown in Fig.2a.

2) Lubricated extrusion where a suitable lubricant is used between the billet, the container and the die Fig.2b.

3) Hydrostatic extrusion in which a fluid layer is under a pressure would deform the material and push it through the die Fig.2c.

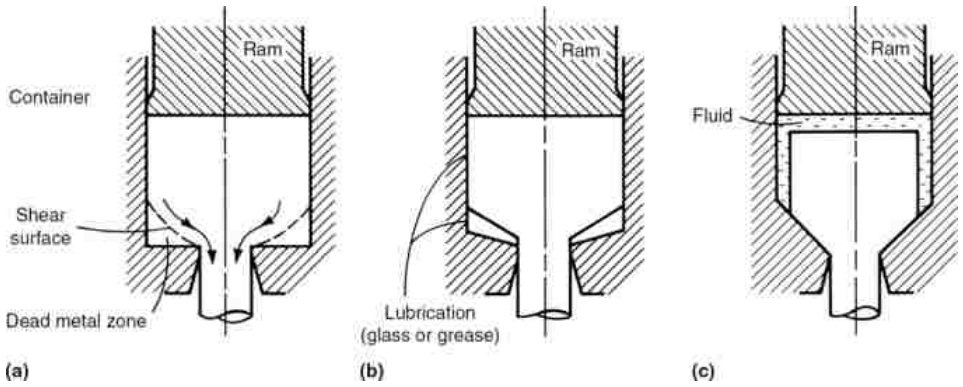

Figure 2. Schematic illustrations showing the major difference between (a) nonlubricated extrusion, (b) lubricated extrusion, and (c) hydrostatic extrusion processes [5]**.**

Based on the relative motion between the billet and the tolling, there are two extrusion types. The first type is direct extrusion where the billet slides into the die with the same direction of the ram as shown in Fig.3a. However, in the indirect extrusion-process, the billet slides in the opposite direction of the ram as shown in Fig.3b. Accordingly, the friction between the container and the billet in the direct extrusion is higher than the indirect extrusion and consequently more energy is required to performed the process.

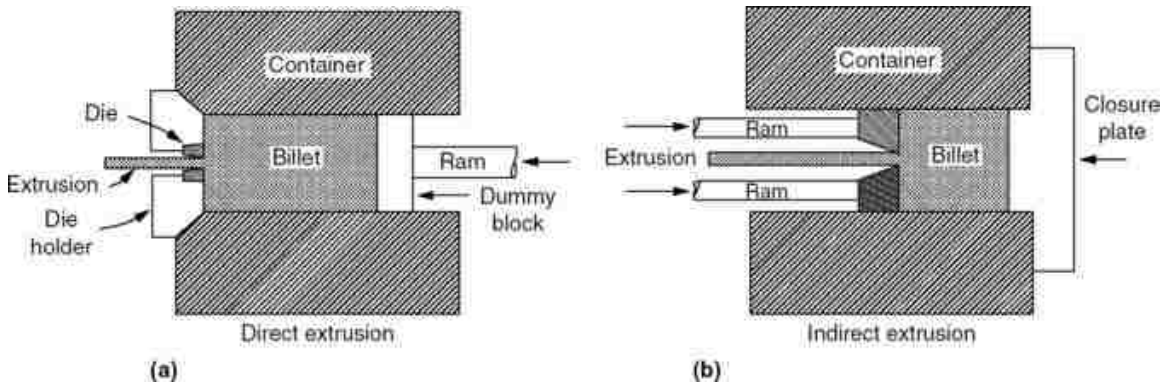

Figure 3. (a) direct extrusion and (b) indirect extrusion[4]

The extrusion process has the ability to produce a good finished complex shapes with a long length, Therefore, many metals are formed by this process such as aluminum, lead, tin, magnesium, zinc, copper, steel, titanium, nickel and others metals and alloys. One of the most ideal material for forming in extrusion is Aluminum and its alloys because of its high ductility of the FCC crystal structure even in low temperature [6]. The most suitable aluminum alloys for extrusion are 1*xxx*, 3*xxx*, 5*xxx*, and 6*xxx* series.

1.5 *Etrudability of Aluminum*

Good extrudibility is a term that described many significant process variable such as high extrusion speed, low extrusion load, decreasing the defects, good tolerance, long tool life. It is hard to define the extrudability precisely because there are many conditions which affect the extrusion process directly and indirectly. Among these conditions are state of the stress within the deformation zone, friction, strain, strain rate, ram speed, the exit speed, temperature of the billet, composition of the alloy and many more. However, in the literature there are different approaches one of them is plotting the relation between maximum extrusion exit speeds ,preheat billet temperature and extrusion ratio as shown in Fig. 4.

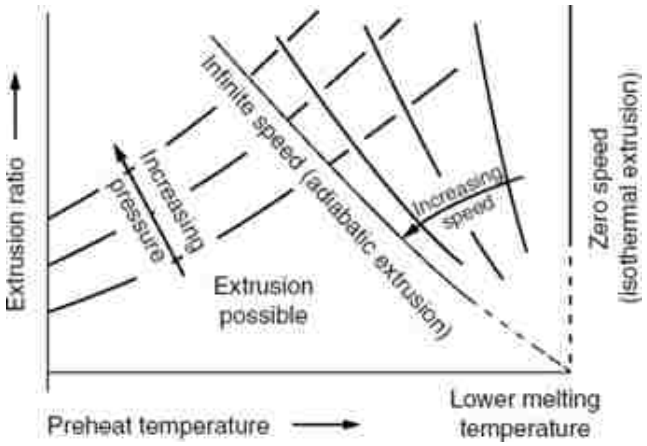

Figure 4. Extrusion exit speed as a function of temperature [6]**.**

Also, Mondolfo and Peel [7] had define the extrusion behavior in two holes die test as shown in Fig.5. The longer the thicker section, the higher is the extrudibilty. Misiolek & Zasadzinski had designed seven holes die test as shown in Fig.6 “which give more possibility to carry out several independent processes simultaneously and thus obtain several rates of metal outflow during the extrusion of a single billet” [8] . In addition, Castle and Lang used a test die and test section to measure the extrudibility with the speed as determinant factor for the quality of the extruded part [7].

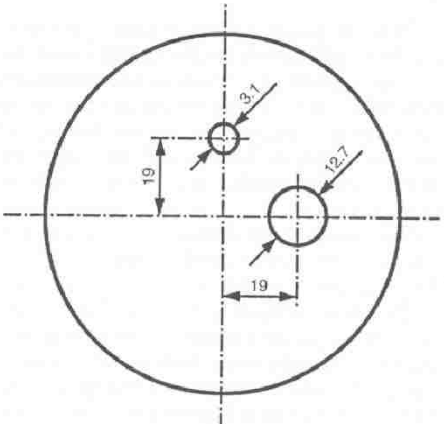

Figure 5. Mondolfo and Peel experimental test die for measuring the extrudibility [7]**.**

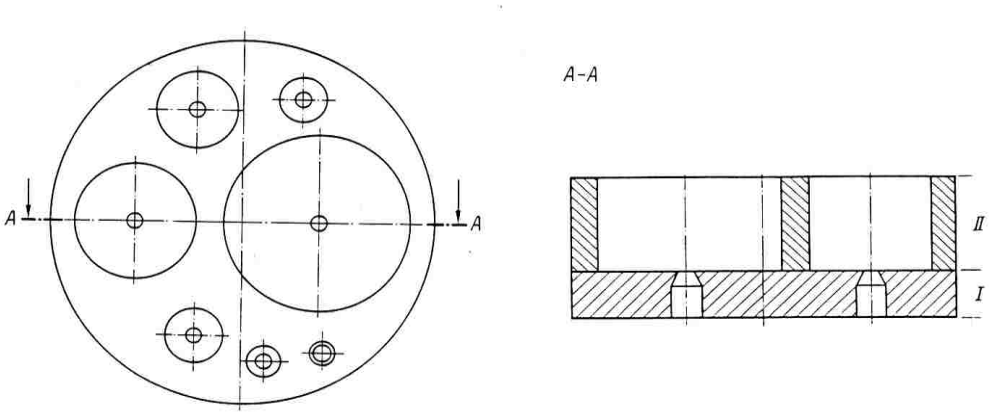

Figure 6.Misiolek & Zasadzinski test die with seven holes [8]**.**

1.6 *Rolling*

Rolling is the process of plastically deforming material by passing it between rolls. It is the most widely used metalworking process because of its high production and close control of geometrical tolerances of the final product. In rolling, the metal is subjected to compressive stresses from squeezing action of the rolls on the metal. The frictional force is drawing the metal into the gap between the working rolls [9].

In another definition, rolling is a deformation process in which the thickness of the work is reduced by compressive forces exerted by two rolls . The rolls rotate to pull and simultaneously squeeze the work between them[10].

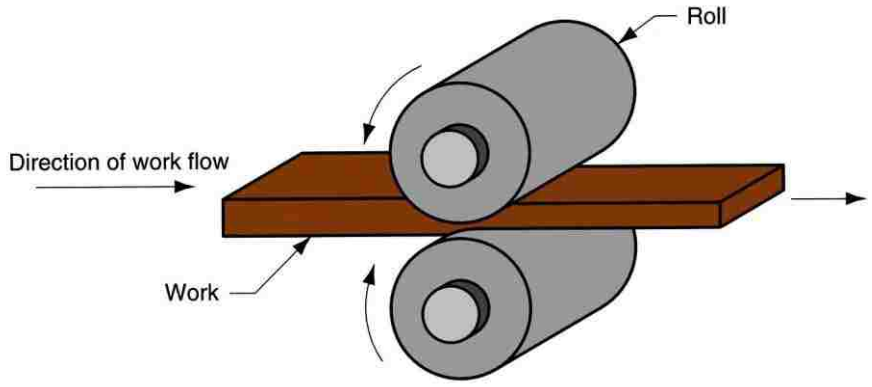

Figure 7. The flat rolling process [10]

1.7 *History of Rolling*

Rolling of gold and silver is known from the 14th century. Leonardo da Vinci designed the first rolling mills in 1480. By around 1600, lead and tin was cold rolled by manually rolling mills. In Europe, iron bars were rolled to sheets in the 18th century. Later, the modern rolling started from 1783 when England issued patent for using grooved rolls to produce the iron bars. The first rolling mill was for I-beam for railway in 1820. In fact, the rolling require more energy so, it was driven by water and then by steam engine until the invention of the electric motor[10].

1.8 *Rolling Mills*

Different designs of the rolling mills have been developed over the years and they can be classified into various types of Rolling [10]

- Based on workpiece geometry :
  - Flat rolling - used to reduce thickness of a rectangular cross section.
  - Shape rolling – a square cross section is formed into a shape such as an I-beam.
- Based on work temperature :
  - Hot Rolling – where the work is above the recrystallization temperature- most common due to the large amount of deformation required
  - Cold rolling – where the work is done below the recrystallization temperature -produces finished sheet and plate stock

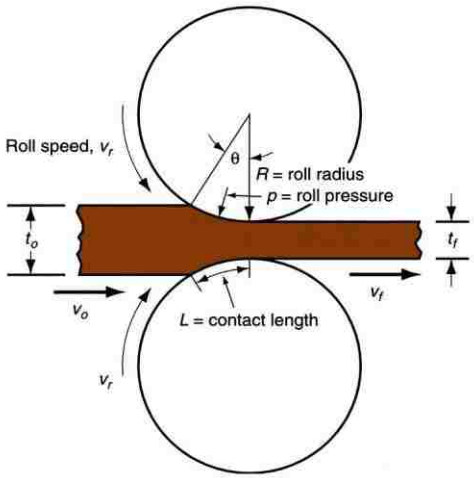

t_o: *starting thickness*
t_f: *final thickness*
v_o: *entering speed of the workpiece*
v_r: *roll speed*
v_f: *final speed of the workkpiece*

Figure 8. Side view of flat rolling, indicating before and after thicknesses, work velocities, angle of contact with rolls, and other features[10]**.**

Rolling mills consist of rolls, bearing, a housing for containing these parts and drive motor for applying the required power.

- Rolling mill configurations:
  - Two-high – two opposing rolls.
  - Three-high – workpiece passes through rolls in both directions.
  - Four-high – backing rolls support smaller working rolls.
  - Cluster mill – multiple backing rolls for smaller working rolls.
  - Tandem rolling mill – sequence of two-high mills.

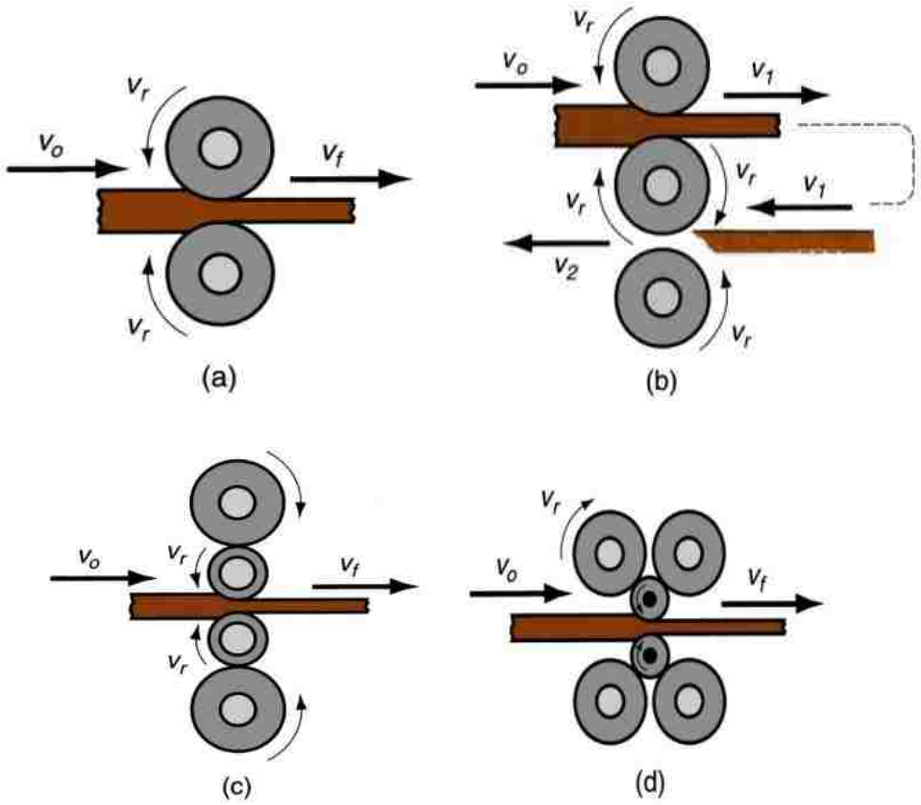

Figure 9. Various configurations of rolling mills (a) 2-high rolling mill. (b) 3-high rolling mill. (c) four-high rolling mill. (d) cluster mill [10]**.**

2 CHAPTER 2: Surface Grain Structure Evolution in AA6082 Hot Direct Extrusion

As a Part of prepared paper : Modeling Surface Grain Structure Evolution in AA6082 Hot Direct Extrusion, Luigi De Pari Jr., Nabeel H. Alharthi Andreas Jäger, Ahmet Güzel, William Van Geertruyden, Marco Schikorra, Wojciech Z. Misiolek, A. Erman Tekkaya. To be submitted to Acta Materialia

2.1 *Introduction*

Peripheral coarse grains (PCG) structure is one of the common defects that appears in the hot deformed aluminum alloys see Fig.10 as a result of a post-dynamic recrystallization phenomenon .The PCG is a large recrystallized grain appears in the circumference or the peripheral of the deformed workpiece. Due to the Hall-Petch effect, the region that contains PCG will have lower mechanical properties in comparison to the whole deformed part. Also, PCG will lead to lower corrosion resistance [11]. For consistent mechanical properties, the manufacturers are spending more cost to remove this defects and consequently, will increase the cost of the products. Therefore, the understanding of the degree of the dynamic recrystallization is very important in predicting PCG.

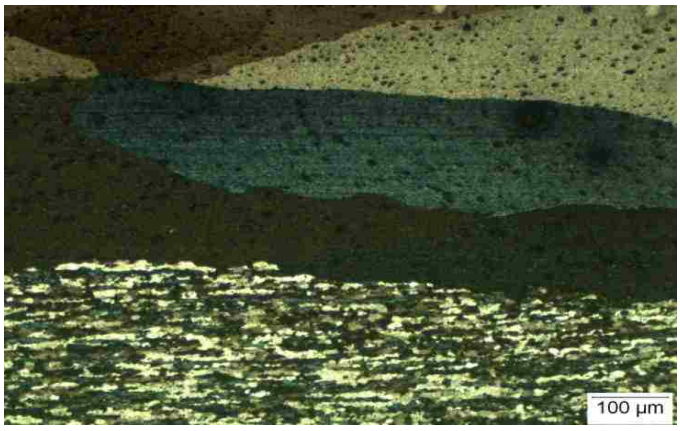

Figure 10. Peripheral Coarse Grains (PCG) in hot AA 6082 extrudate.

There are two mechanisms of dynamic recrystallization in high stacking fault energy material such as aluminum reported in literature [12-15]. The first one is the continuous dynamic recrystallization (CDRX) and the second is geometric dynamic recrystallization (GDRX). CDRX occurs by the accumulation of dislocations into cell walls which will form a substructure of low-angle grain boundaries (LAGBs). With enough dislocation accumulation, the boundary misorientation and LAGBs transform to high angle grain boundaries (HAGBs) and small grain are formed [16].

In GDRX, the original grains are elongated by deformation. At enough strain the original grains thickness is reduced to almost 2 subgrains diameter. Consequently, subgrains are formed and suddenly, the subgrains is pinched-off resulting in new small equiaxed grains Fig. 11.

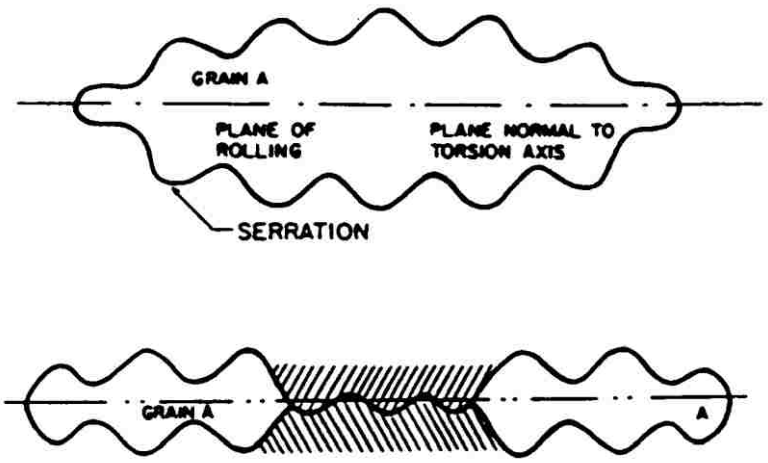

Figure 11 When the grains are elongated and thinned extremely, they pinch off where opposite serrations meet and form new grains by GDRX mechanism [17]

DePari and Misiolek have developed a new joint DRX model that considers both CDRX and GDRX to predict the surface microstructure evolution (i.e., grain diameter, subgrain diameter, and grain boundary misorientation) of aluminum alloy 6061 during a hot-torsion test and hot-rolling [18] as a function of the state variables: strain, strain rate, temperature, and stress. Later, they used the same model to predict the surface microstructure evolution in AA 6082 hot extrudate to check the validity of the model [16]. Also, They have verified the model experimentally by characterization of AA 6082 extrdate [16][18]. However, one ram speed hot extrudate sample (1 mm/sec) has been verified.

The objective of constructing the DRX model is to give the suppliers of the deformed material an information about the surface physical properties of their products depending on a state variables During deformation, the state variables can be obtained from a different software simulation package such as DEFORM^{TM}, QFORM^{TM} LS-DYNA^{TM}, FORGE^{TM} and others.

In this work, four different ram speeds (0.25, 0.5, 2, 5 mm/sec) in hot extrusion were investigated in terms of surface microstructure evolution (i.e. grain size and misorintation angle. Also, numerical modeling package DEFORM^{TM} -3D was used to simulate the hot extrusion for AA 6082. After that, the state variables results which were obtained from DEFORM^{TM} -3D were plugged in the Joint DRX model to predict the surface grain size for different ram speeds.

2.2 *AA6082 Hot Direct Extrusion*

An aluminum alloy AA6082 (Al-Mg-Si) was analyzed as shown in Fig.12 .The geometry is a double symmetric solid profile with a wall thickness of 3 mm in the center increasing up to 15 mm to the sides by a main diagonal of 70 mm

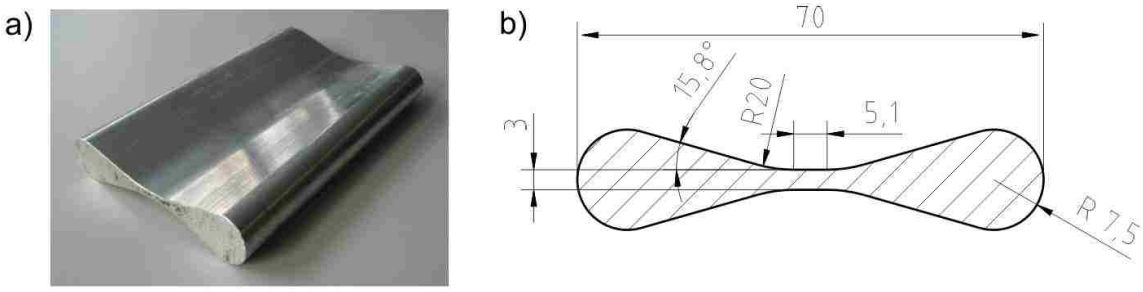

Figure 12. (a) General view of the extrusion specimen (b) Cross-section of the extruded profile

Extrusion was performed on a 10 MN direct extrusion press with a flat die, which had a constant bearing length equal to 15 mm. Direct-chilled cast and homogenized billets with dimensions of 140 mm (diameter) 300 mm (length) were used with a container of 146 mm in diameter. The extrusion ratio 26.3. This extrusion was performed in high temperature up to 537°C which was measured by a thermocouple in the surface of the billet. Also, the ram speeds were set to 0.25, 0.5, 2, 5 mm/sec, which resulted in exiting speeds of 6.57, 13.15, 52.6, 131.5 mm/sec respectively. Immediately, after initiation of the process in a distance of 250 mm from the die exit, a quenching was applied. The quenching apparatus consisted of two pairs of air atomizing nozzles mounted above and below the extrudate. This arrangement was chosen to avoid the static recrytalization and to keep the extrudate under slow cooling conditions which over-

locked the microstructure as under dynamic recrystallization during the extrusion Fig 13

.

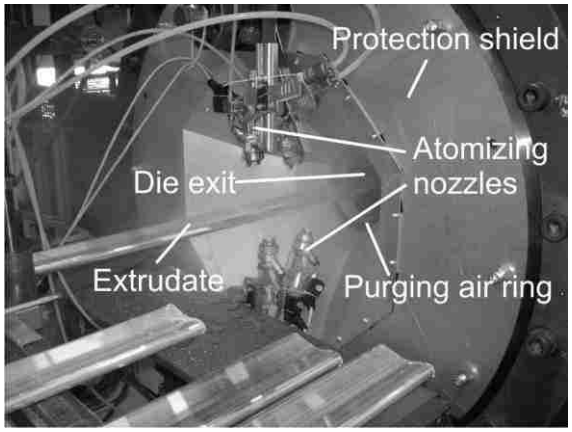

Figure 13. Experimental setup for the extrusion of AA6082

2.3 *Sample preparation for Light Optical Microscopy (LOM)*

The microstructure of AA 6082 hot extrudate was analyzed at three locations in each sample as shown in Fig.14. The samples were prepared using the following procedures:

1- Cutting the samples by using Isomet low speed Buehler saw with diamond wheel.

2- Mounting the samples in Epoxy with cylindrical shape.

3- Grinding samples by using silicon carbide papers 320, 400, 600 and 800 µm respectively and water as coolant. Each sample were ground for one minute.

4- Polishing samples with diamond 6, 3, 1 µm respectively and the final polishing with silicon dioxide.

5- Electroetching samples with 30 V for 60 to 90 sec immersed in Barker's (Tetrafluoroboric Acid 48%) 3% in distilled water.

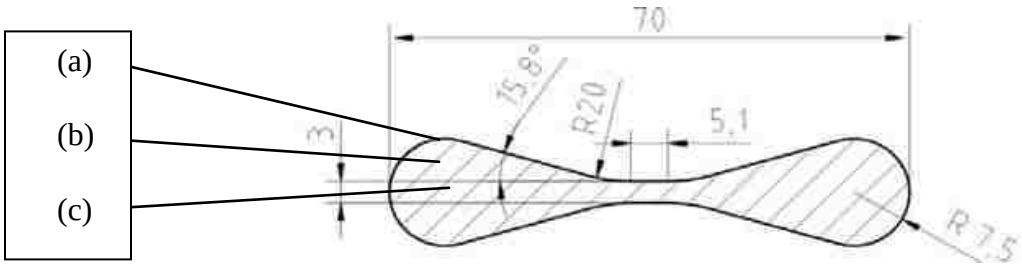

Figure 14, Schematic drawing for the sample which shows where the LOM images were taken

2.4 *Images from LOM*

After sample preparation, Nikon light optical microscopy was used to analyze the microstructure of four samples in three different locations as shown in Fig.14. Each sample was represented a part extruded with specific ram speed. All LOM images were polarized. The following images represent the microstructure for each location for each part .

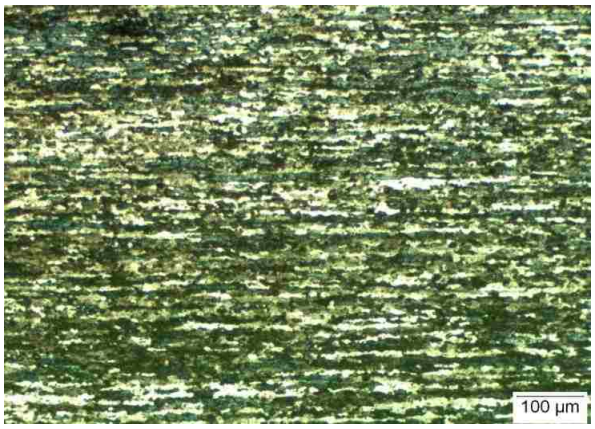

(a)

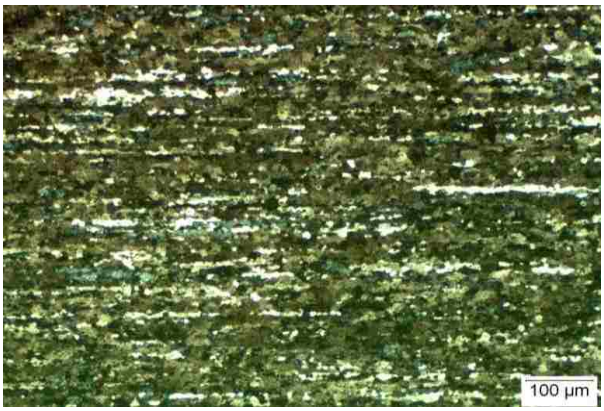

(b)

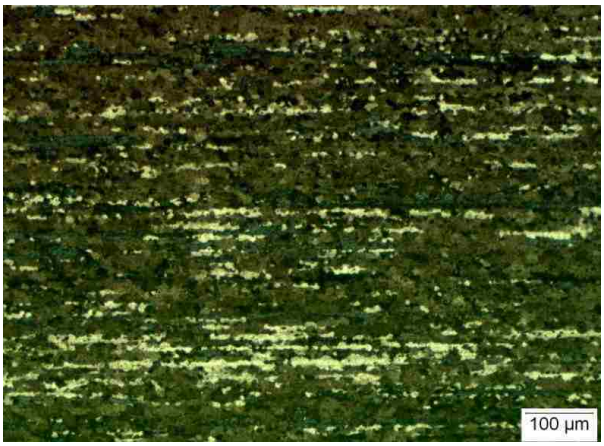

(c)

Figure 15. Light Optical Microscopy images for the thickest part of the extrudate extruded with the ram speed 0.25mm/sec (a) top (b) center (c) middle

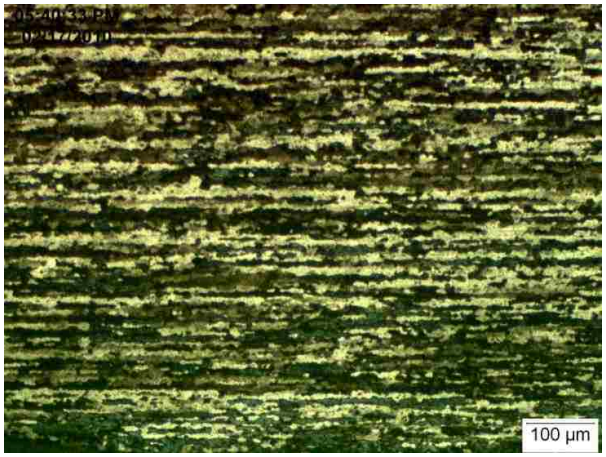

(a)

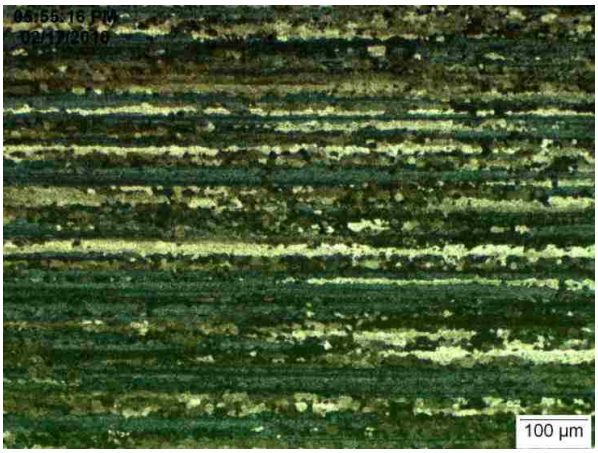

(b)

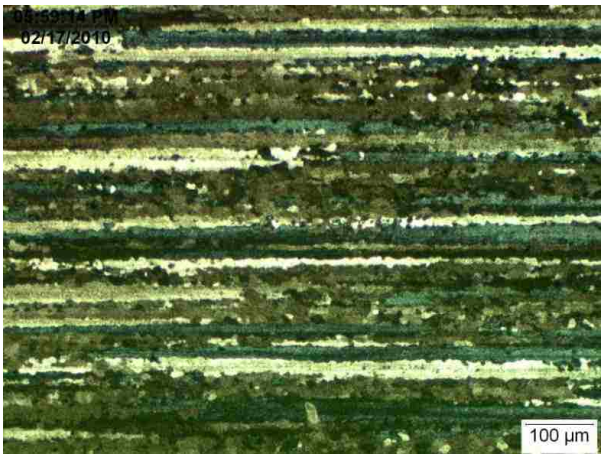

(c)

Figure 16. Light Optical Microscopy images for the thickest part of the extrudate extruded with the ram speed 0.50mm/sec (a) top (b) center (c) middle

(a)

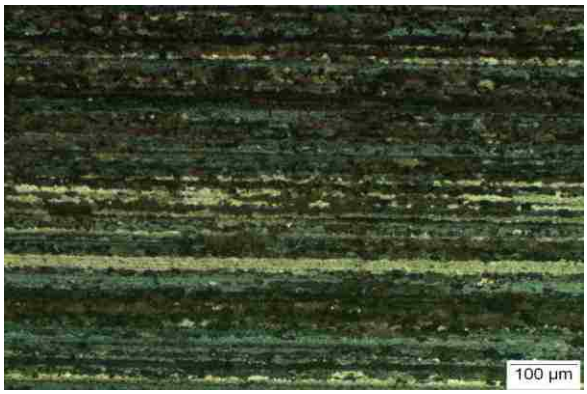

(b)

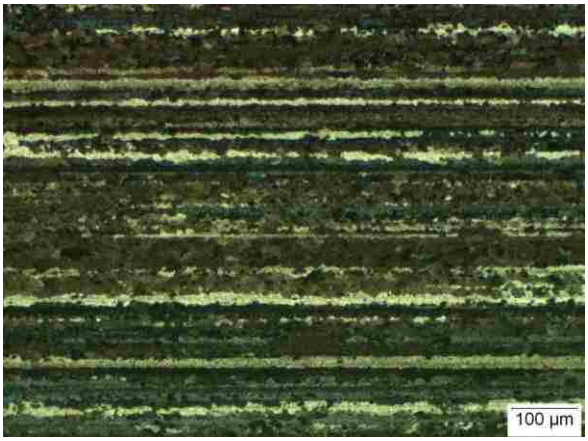

(c)

Figure 17. Light Optical Microscopy images for the thickest part of the extrudate extruded with the ram speed 2mm/sec (a) top (b) center (c) middle

(a)

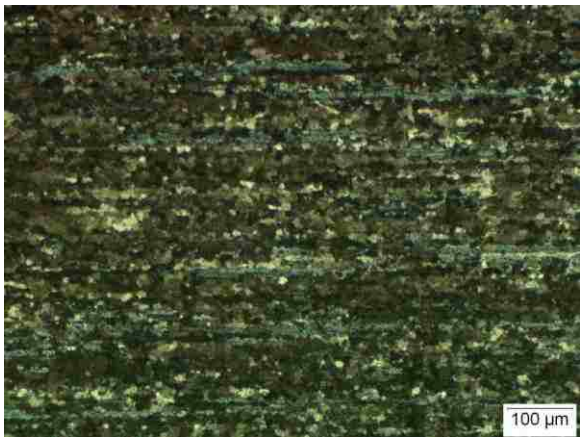

(b)

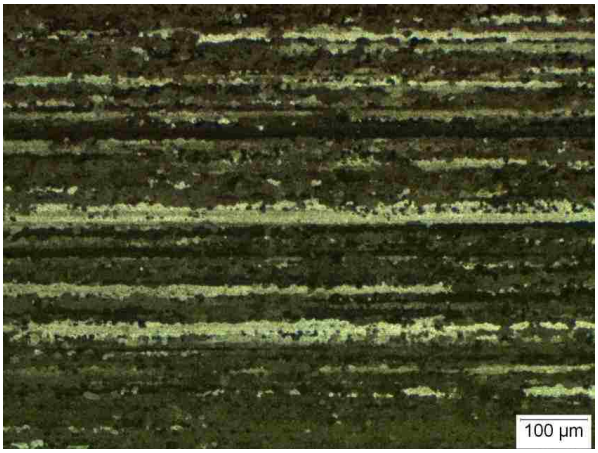

(c)

Figure 18. Light Optical Microscopy images for the thickest part of the extrudate extruded with the ram speed 5mm/sec (a) top (b) center (c) middle

2.5 *Sample preparation for Electron Backscatter Diffraction (EBSD)*

Samples of AA 6082 hot extrusion were prepared for EBSD analysis by the following procedures:

1- Cutting the samples and mounted in epoxy mounts.

2- Grinding samples by using silicon carbide papers 320, 400, 600 and 800 µm respectively and water as coolant. Each sample were ground for one minute.

3- Polishing samples with diamond 6, 3, 1 µm respectively then with silicon dioxide.

4- Final polishing with 0.5 µm SiO_2 to eliminate any aluminum oxide layer.

5- chemical polish solution which is comprised of: 70% (H_3PO_4) Phosphoric Acid, 25% (H_2SO_4) Sulfuric Acid, and 5% (HNO_3) Nitric Acid . The solution was heated to 85ºC and the samples were dipped in the solution for approximately 20s [19]

Because of the difficulty in measuring the grain size with the light optical microscopy technique, the EBSD was used to measure the grain size and the misoriantation angle fraction at the surface of the thickest part of the extrudate as shown in Fig. 19.

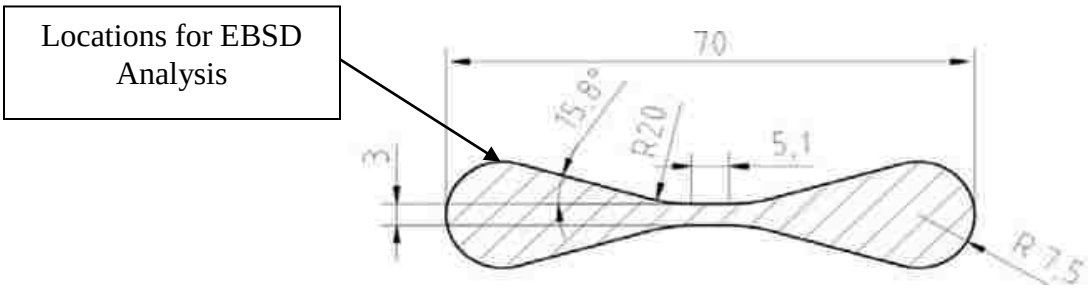

Figure 19. Schematic drawing illustrating where the EBSD analysis was performed

2.6 *EBSD analysis results*

Four samples were analyzed using EBSD in Hitachi S-4300 SEN. The EBSD images were taken as shown in Fig.19. In the following sections and for every ram speed extrudate, the EBSD images were posted with the directions and inverse pole figures which map the orientation of the grains. Also, the grain size distribution with the area fraction are plotted. In addition, the fraction of low angle grain boundaries histograms are plotted which show the misoriantaion angle versus the number of fraction.

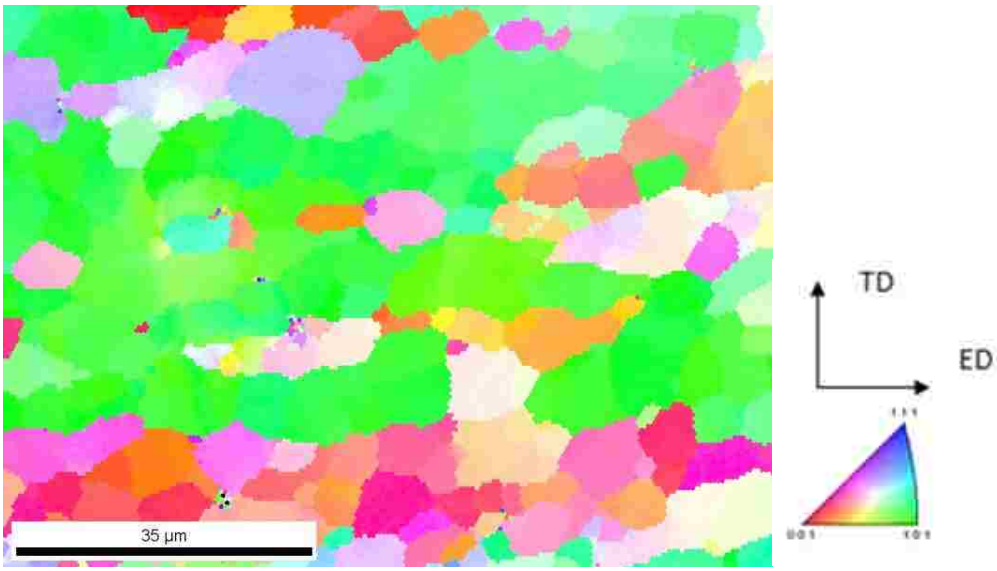

Figure 20. EBSD image for a part extruded with ram speed 0.25 mm /sec

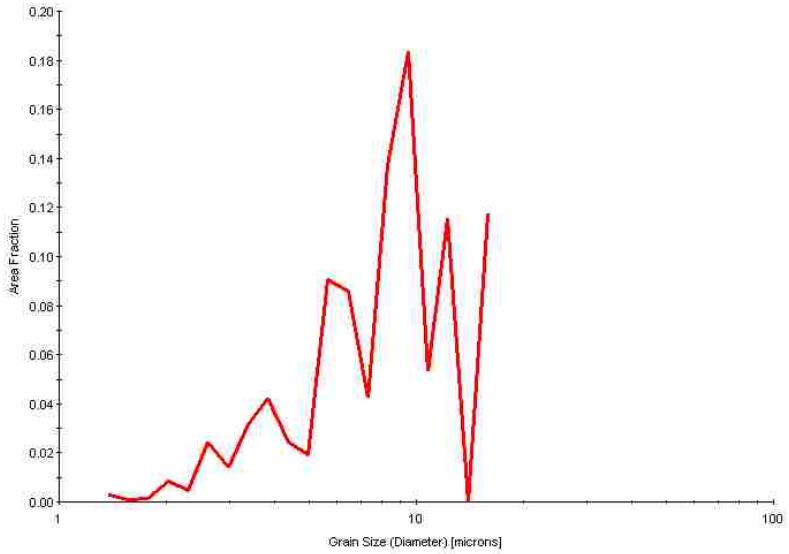

Figure 21. Area fraction of grain size for a part extruded with ram speed 0.25mm/sec

Table 2. Area fraction of the grain size for a part extruded with ram speed 0.25mm/sec

Chart: Grain Size (diameter)

Edge grains excluded from analysis

Diameter [microns]	Area Fraction
1.37166	0.00293852
1.5603	0.000904159
1.77488	0.00124322
2.01898	0.00847649
2.29664	0.0045208
2.61249	0.0246383
2.97178	0.0142405
3.38048	0.0316456
3.84538	0.0423825
4.37423	0.0245253
4.9758	0.0192134
5.66011	0.0905289
6.43852	0.0861212
7.32399	0.0422694
8.33123	0.136867
9.477	0.183544
10.7803	0.0531194
12.2629	0.115393
13.9494	0
15.8678	0.117428

Average	
Number	4.90181
Standard Deviation	3.08458
Area	8.80512

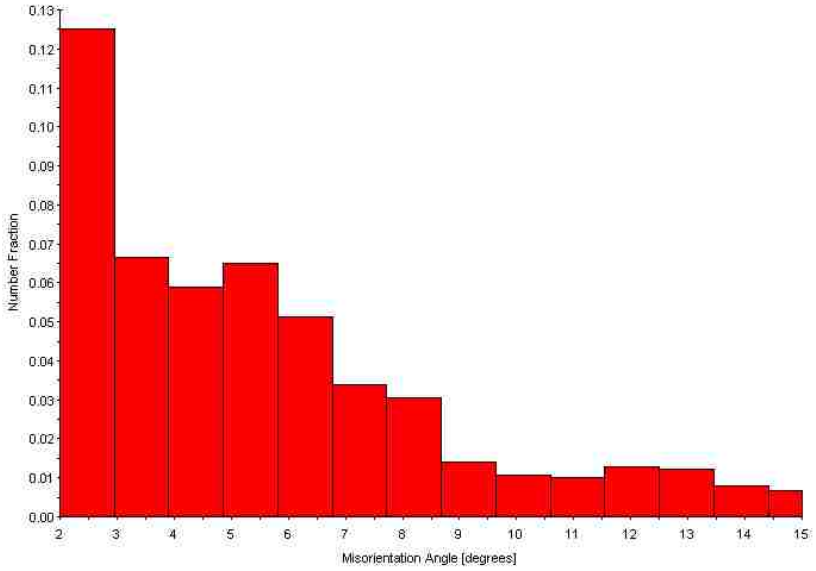

Figure 22. The fraction of LAGB for a part extruded with ram speed 0.25 mm/sec

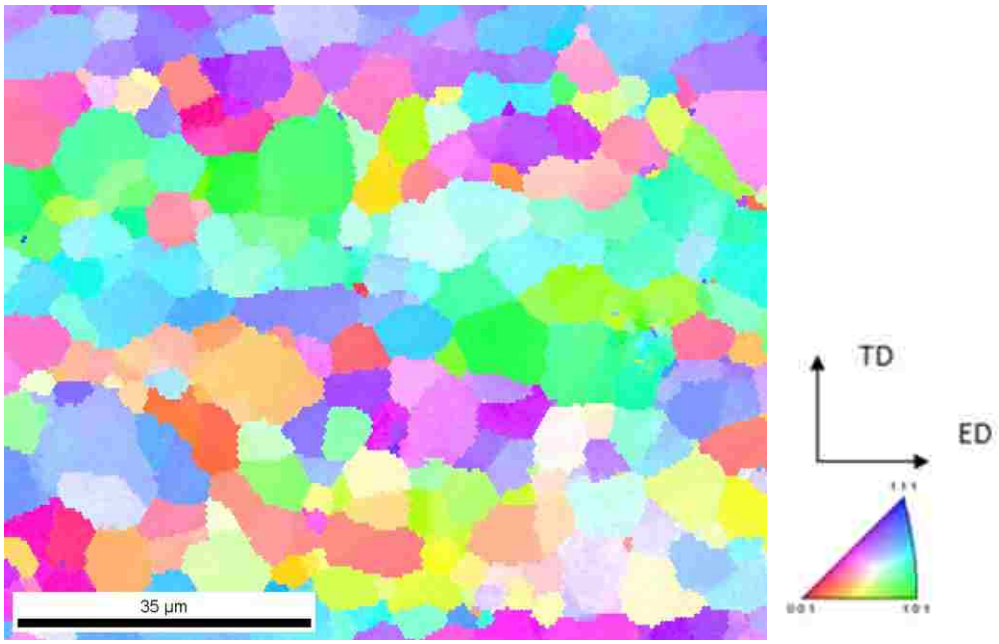

Figure 23. EBSD image a part extruded with ram speed 0.5 mm /sec

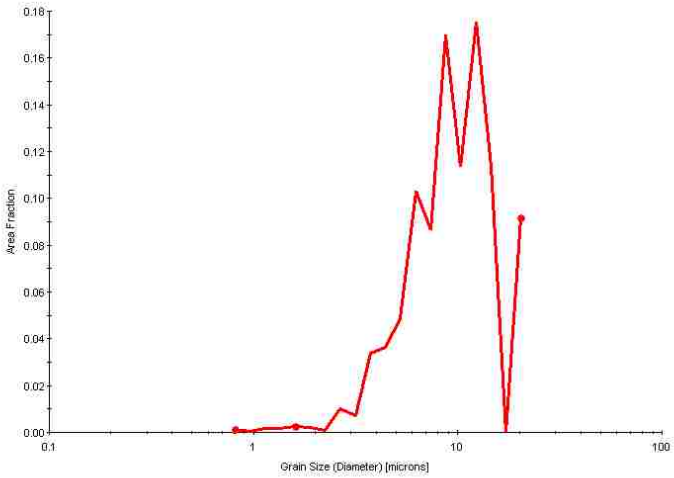

Figure 24. Area fraction of grain size for a part extruded with ram speed 0.5mm/sec

Table 3. Area fraction of the grain size for a part extruded with ram speed 0.5mm/sec

Chart: Grain Size (diameter)

Edge grains excluded from analysis

Diameter [microns]	Area Fraction
0.80834	0.00133463
0.958013	0.000307992
1.1354	0.00153996
1.34563	0.00169396
1.59479	0.0027206
1.89008	0.00195062
2.24005	0.000975309
2.65482	0.00995842
3.14639	0.00718649
3.72898	0.0336738
4.41944	0.0361891
5.23775	0.0486115
6.20758	0.103075
7.35698	0.0867512
8.71921	0.16996
10.3337	0.113239
12.2471	0.175248
14.5147	0.113855
17.2023	0
20.3875	0.0917304
Average	
Number	5.12136
Standard Deviation	3.81648
Area	10.3664

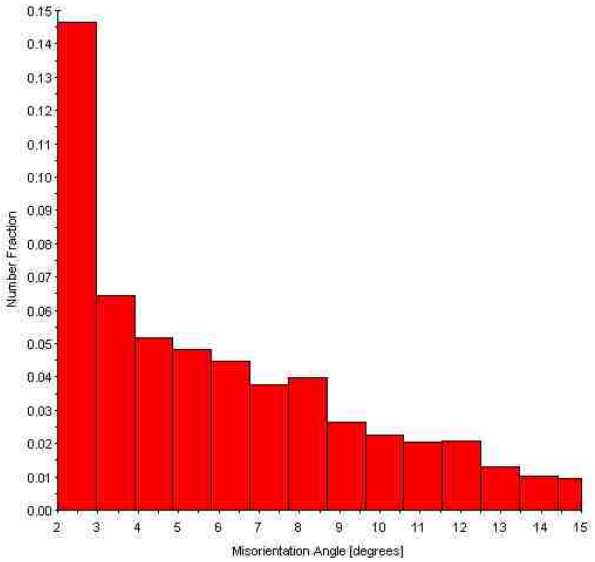

Figure 25. The fraction of LAGB for a part extruded with ram speed 0.5 mm/sec

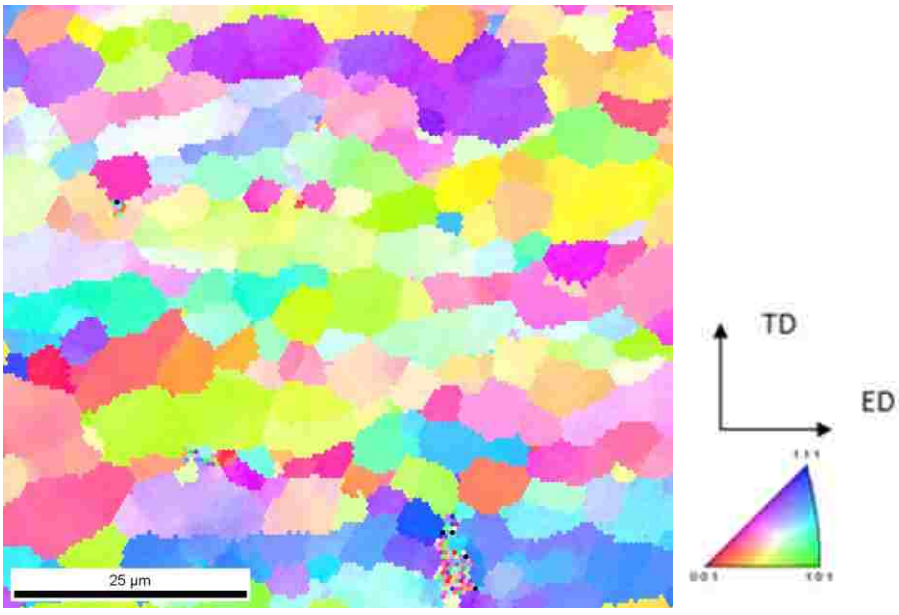

Figure 26. EBSD image for a part extruded with ram speed 2 mm /sec

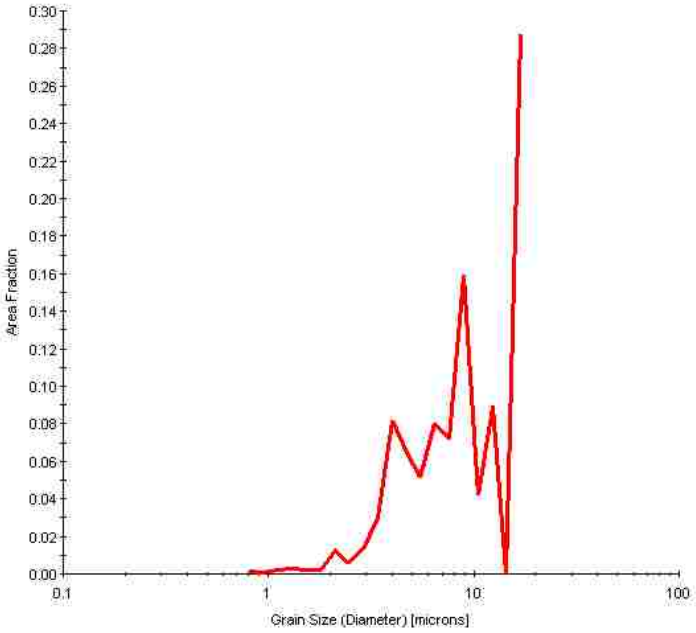

Figure 27. Area fraction of grain size for a part extruded with ram speed 2 mm/sec

Table 4. Area fraction of the grain size for a part extruded with ram speed 2 mm/sec

Chart: Grain Size (diameter)

Edge grains excluded from analysis

Diameter [microns]	Area Fraction
0.804493	0.00142526
0.944398	0.00080171
1.10863	0.00187066
1.30143	0.00285053
1.52776	0.00231605
1.79345	0.00195974
2.10534	0.0130055
2.47147	0.00561197
2.90127	0.0134509
3.40582	0.029396
3.99811	0.0817745
4.6934	0.0645822
5.50961	0.0513095
6.46776	0.0804383
7.59255	0.0720648
8.91293	0.159095
10.4629	0.0414217
12.2825	0.0893462
14.4185	0
16.926	0.28728
Average	
Number	4.26842
Standard Deviation	3.45561
Area	10.1061

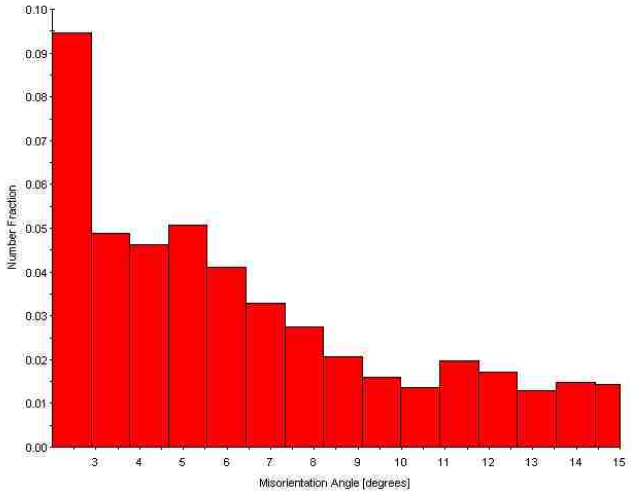

Figure 28. The fraction of LAGB for a part extruded with ram speed 2 mm/sec

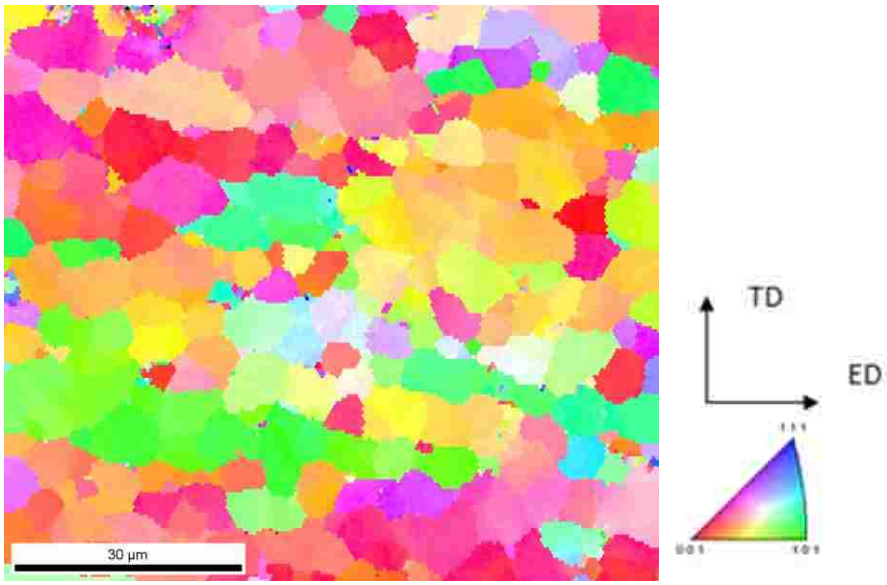

Figure 29. EBSD image for a part extruded with ram speed 5 mm /sec

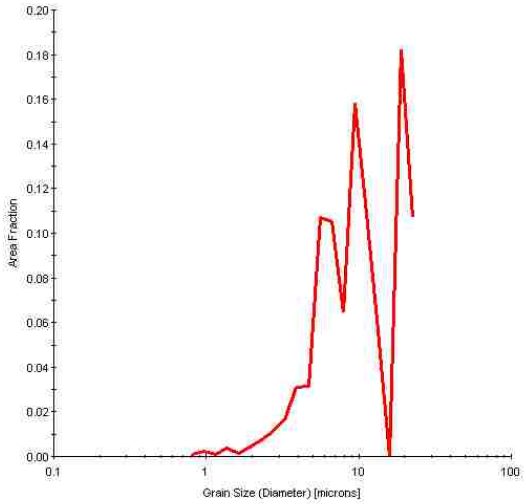

Figure 30. Area fraction of grain size for a part extruded with ram speed 5mm/sec

Table 5. Area fraction of the grain size for a part extruded with ram speed 5mm/sec

Chart Grain Size (diameter)

Edge grains excluded from analysis

Diameter [microns]	Area Fraction
0.810407	0.000974849
0.96538	0.00219341
1.14999	0.000974849
1.3699	0.00385065
1.63186	0.00155976
1.94392	0.00424059
2.31566	0.00760382
2.75848	0.0110645
3.28598	0.01628
3.91436	0.0310489
4.6629	0.0315364
5.55458	0.107185
6.61677	0.10504
7.88209	0.0640963
9.38938	0.158169
11.1849	0.108842
13.3238	0.0562975
15.8717	0
18.9068	0.182199
22.5223	0.106843
Average Number	4.71417
Standard Deviation	3.94766
Area	11.6256

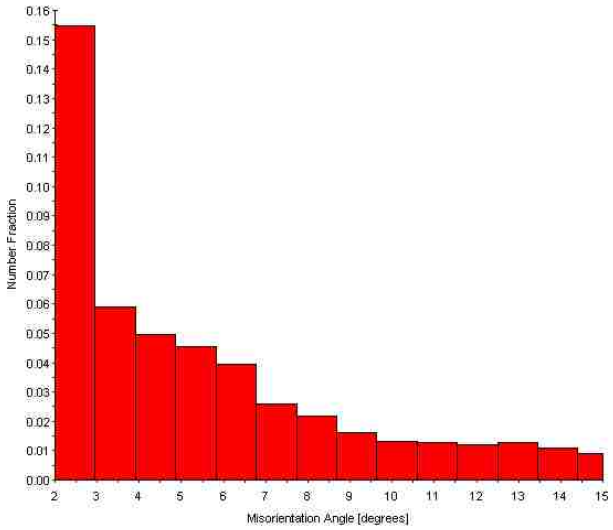

Figure 31. The fraction of LAGB for a part extruded with ram speed 5 mm/sec

The EBSD analysis results were summarized in Table 6. These results are verification for with the model results presented in the discussion section.

Table 6. Average grain size in μm and the fraction of LAGBs for all the extruded parts with different ram speeds

Ram Speed	Avg. Grain Diam., D_f (μm)	Fraction of LAGBs, f_{LAGB}.
0.25 mm/sec	4.9	0.4489
0.5 mm/sec	5.12	0.5656
2 mm/sec	4.268	0.5065
5mm/sec	4.71	0.4948

2.7 *AA6082 Hot-Direct Extrusion simulation*

The simulation of the extrusion process was done by using the finite element-modeling package DEFORM^{TM} -3D to obtain the localized state variables of temperature, strain, strain rate, and stress . The initial conditions for the simulation are in table 7. Then, the localized state variables from DEFORM^{TM} -3D were used in MATLAB codes which were written by Luigi De Pari Jr[16].

Table 7. Initial condition for the DEFORM^{TM} -3D simulation of analyzed extrusion

Billet Diameter	140 mm (5.51 in)
Billet Temperature	537 ^{o}C (999 ^{o}F),
Extrusion Ratio	26.3
Die Temperature	380 °C (716 ^{o}F)
Container Temperature	450 °C (842 ^{o}F)
Ram Temperature	450 °C (842 ^{o}F)
Ram Speed	0.25, 0.5, 1, 2 & 5 mm/sec
Heat Transfer Coefficient (Billet - Die)	11000 W/(m^2 ^{o}C) 0.538 Btu/(s ft^2 ^{o}F))
Heat Transfer Coefficient (Billet - Container)	11000 W/(m^2 ^{o}C) 0.538 Btu/(s ft^2 ^{o}F))
Heat Transfer Coefficient (Billet - Ram)	11000 W/(m^2 ^{o}C) 0.538 Btu/(s ft^2 ^{o}F))
Time Step	Varying (max 0.0025 sec)
Die Shear Friction Coefficient	0.5
Container Shear Friction Coefficient	0.9
Ram Shear Friction Coefficient	0.9

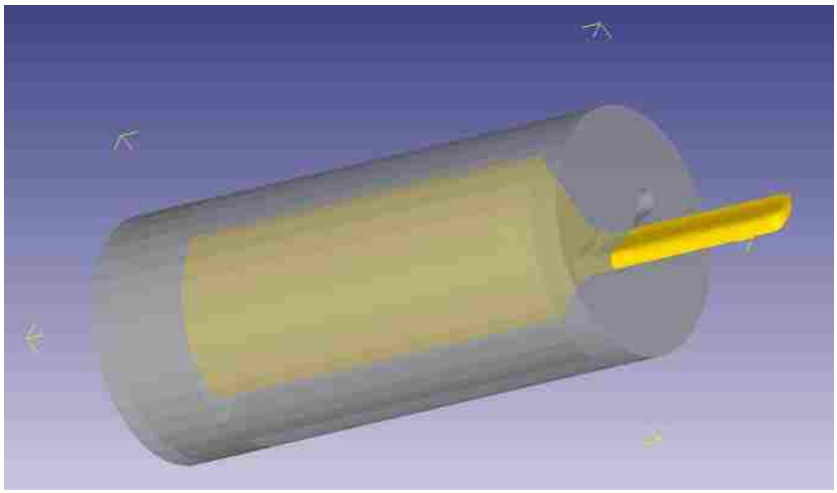

Figure 32. Image of the DEFORM™ –3D simulation for the hot extrusion of AA 6082

2.8 *Simulation Results*

The models were coded as a MATLAB codes and were run. The results of the prediction of the average grain size and the fraction of LAGBs for three different models Joint DRX, CDRX and GDRX were summarized as shown in Table 8.

Table 8. The Joint DRX, CDRX, GDRX models average grain diameter, D_f and fraction of LAGB (f_{LAGB})

Ram Speed	Measured Item	Model		
		Joint DRX	CDRX	GDRX
0.25 mm/sec	Avg. Grain Diam., D_f (μm)	8.16	8.18	4.04
	Fraction of LAGBs, f_{LAGB}	0.5898	0.6	0.7609
0.5 mm/sec	Avg. Grain Diam., D_f (μm)	9.06	8.99	3.472
	Fraction of LAGBs, f_{LAGB}	0.5724	0.5843	0.777
2 mm/sec	Avg. Grain Diam., D_f (μm)	7.37	7.47	3.57
	Fraction of LAGBs, f_{LAGB}	0.5873	0.5974	0.6589
5mm/sec	Avg. Grain Diam., D_f (μm)	7.012	7.088	3.02
	Fraction of LAGBs, f_{LAGB}	0.5580	0.5632	0.684

The following graphs is showing the comparison between the different three models prediction of the grain size and the experimental results.

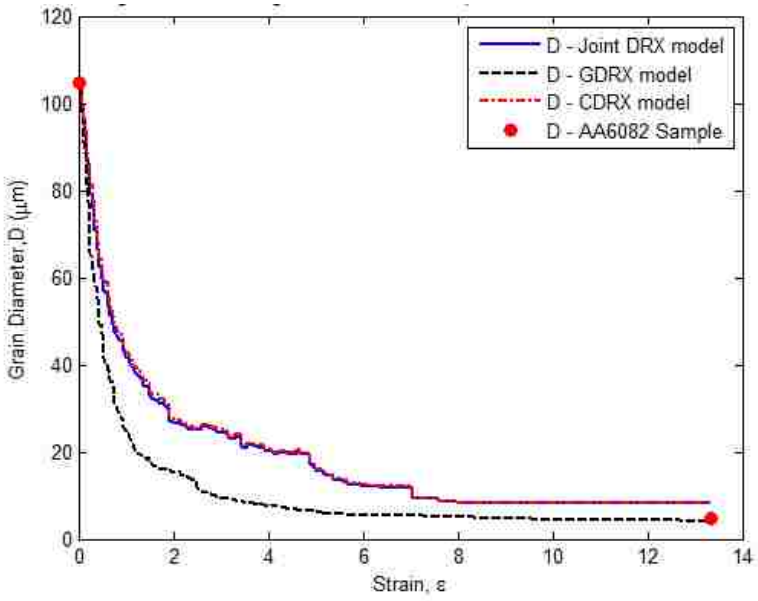

Figure 33. Joint DRX, GDRX, CDRX, and experimental results for average grain diameter at the surface for AA6082 hot-direct extrusion for different ram speed 0.25 mm/sec

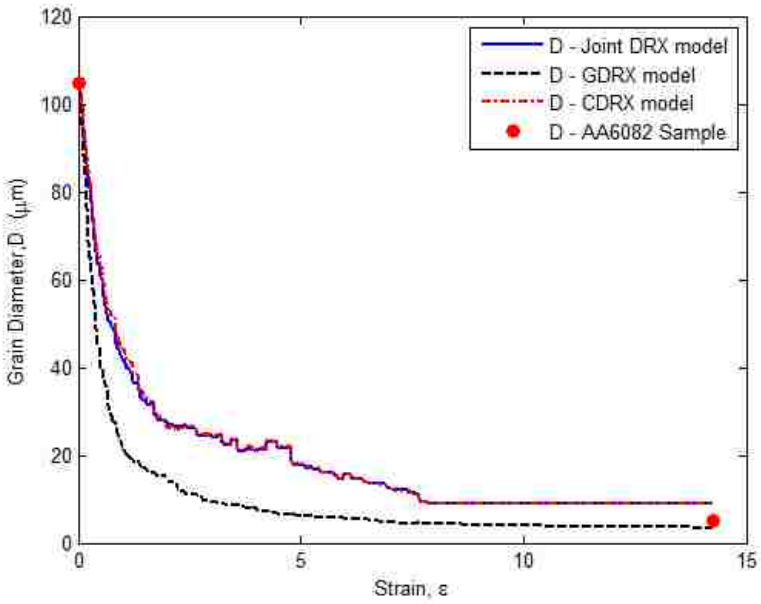

Figure 34. Joint DRX, GDRX, CDRX, and experimental results for average grain diameter at the surface for AA6082 hot-direct extrusion for different ram speed 0.5 mm/sec

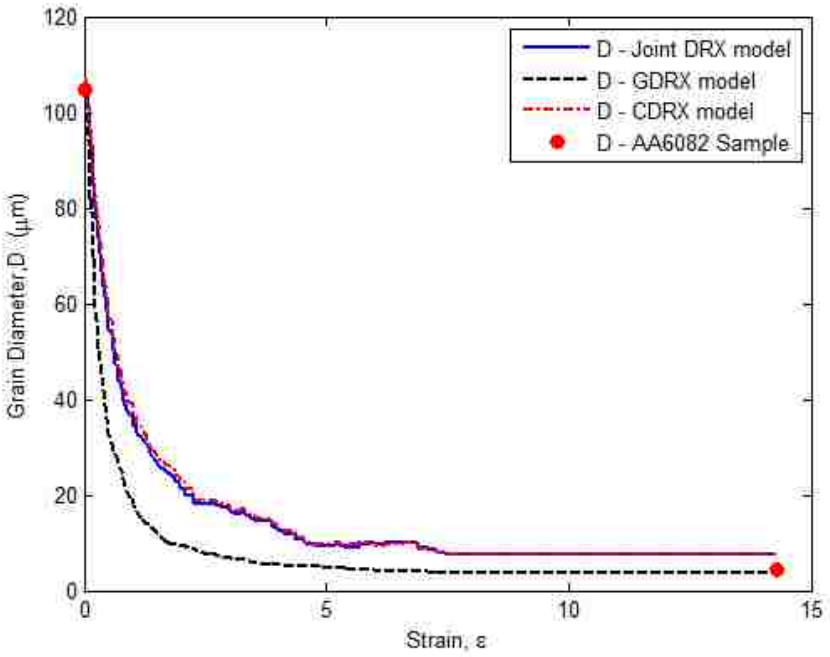

Figure 35. Joint DRX, GDRX, CDRX, and experimental results for average grain diameter at the surface for AA6082 hot-direct extrusion for different ram speed 2mm/sec

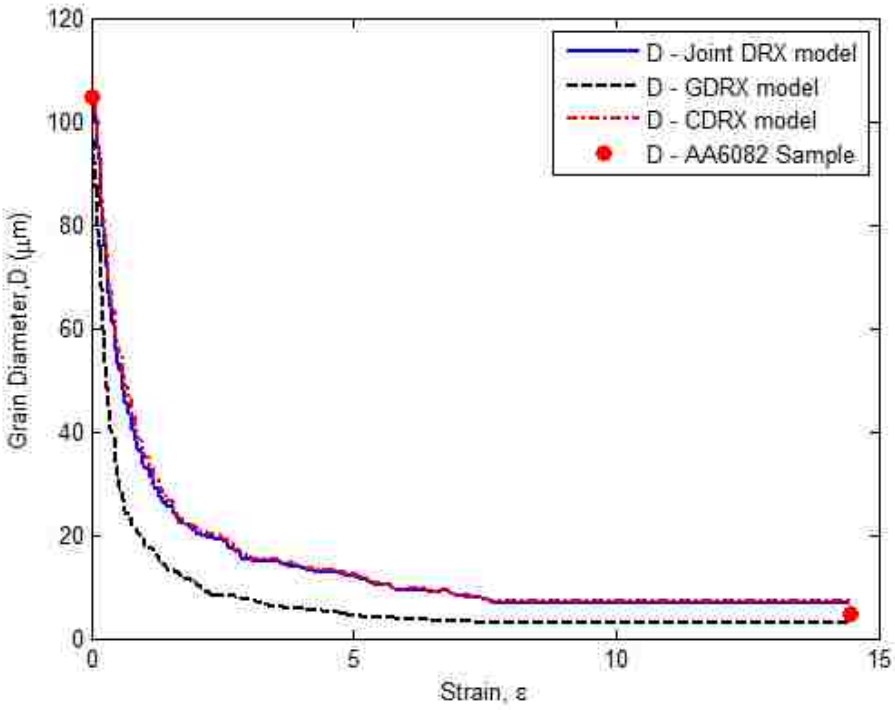

Figure 36. Joint DRX, GDRX, CDRX, and experimental results for average grain diameter at the surface for AA6082 hot-direct extrusion for different ram speed 5 mm/sec

2.9 *Discussion*

The main objective of this work was to verify the Joint DRX model by characterizing and evaluating AA 6082 hot extruded parts. These parts were extruded in different ram speeds. Definitely, the variation of the ram speeds was resulted to different deformation behavior. Consequently, material behaved differently in terms of grain diameters and misorientation angle . Also, the experimental work was provided a good connection between the microstructure at the surface of the extruded part with the state variables that were obtained from the finite element package DEFORM^{TM} -3D.

2.9.1 Light Optical Microscopy Characterization

The goal of LOM images was to measure the average grain size in the extruded parts. As shown in Fig. 14-18, it was difficult to determine the average grain size from the polarized images. But, these images were provided a qualitative description of the deformed parts. It can be observed that the more fine grain microstructure were located in the locations “a” which were in the thickest section of the extruded part. This a good indication that the material went through sever deformation and the dynamic recrystallization took place. Also, it can be observed the shear bands in the location “b” and “c” because of the easy of the flow throughout the die in these locations. In Fig. 18a, the PCG can be observed in the extruded part with ram speed of 5mm/sec.

2.9.2 EBSD analysis

EBSD was determined the average grain size in the thickest section of the extruded parts and the LAGBs distribution. It can be observed from Figs. 20, 23, 26, 29 and Table 6, that the average grains diameters were between 4 and 5 μm which is considered a fine grain microstructure. Also, from Table 6, the fraction of LAGBs were obtained by calculate the misorientation angles distribution below 15 º. The fraction of LAGBs were ranged from 45% to 56% which would play a role in the dynamic recrystallization [17] and consequently the formation of PCG [19] .

2.9.3 3D simulation and the Joint DRX Model

The results from the experimental work and the predicted models' results for the average grain diameter were compared in Table 9. The results showed that the joint DRX model predicted the fraction of the LAGBs very close in comparison to the experimental work and better than the GDRX alone. However it is very close to the CDRX. This prediction was very important to expect the formation of PCG as mentioned in the previous section.

The average grain diameter was predicted very well by the GDRX alone. On the other hand, the prediction in the joint DRX is better than the CDRX alone. In general, the experimental results showed a good a agreement with the model as shown in Fig. 32-36. The model accuracy was discussed in Luigi Ph.D dissertation [16].

Table 9. Comparison between experimental average grain diameter, *D* and fraction of LAGB (f_{LAGB}) and the Joint DRX, CDRX, GDRX models predictions

Ram Speed		Exp. Values	Joint DRX		CDRX		GDRX	
			Sim.	Diff.	Sim.	Diff.	Sim.	Diff.
0.25 mm/sec	Avg. Grain Diam., D_f (μm)	4.9	8.16	3.26	8.18	3.28	4.04	-0.86
	Fraction of LAGBs, f_{LAGB}	0.4489	0.5898	0.1409	0.6	0.1511	0.7609	0.312
0.5 mm/sec	Avg. Grain Diam., D_f (μm)	5.12	9.06	3.94	8.99	3.87	3.472	-1.648
	Fraction of LAGBs, f_{LAGB}	0.5656	0.5724	0.0068	0.5843	0.0187	0.777	0.2114
2 mm/sec	Avg. Grain Diam., D_f (μm)	4.268	7.37	3.102	7.47	3.202	3.57	-0.698
	Fraction of LAGBs, f_{LAGB}	0.5065	0.5873	0.0808	0.5974	0.0909	0.6589	0.1524
5mm/sec	Avg. Grain Diam., D_f (μm)	4.71	7.012	2.302	7.088	2.378	3.02	-1.69
	Fraction of LAGBs, f_{LAGB}	0.4948	0.5580	0.0632	0.5632	0.0684	0.684	0.1892

From the model predictions and the state variables –stress ,strain, strain rate, and temperature - that were obtained from the finite element package - DEFORM^{TM} -3D, a correlation between the average grain diameter and the fraction of the LAGBs can be made with the state variables directly. This correlation helps to know what the amount of strain rate, stress, and temperature that could cause the fine grain microstructure and consequently the formation of the PCG by DRX. Also, by the verification from the experimental work, the manufacturers of the deformed materials could built data base for their final product to eliminate the expected PCG that could be formed during the manufacturing process and maintain good specifications their product Fig.37.

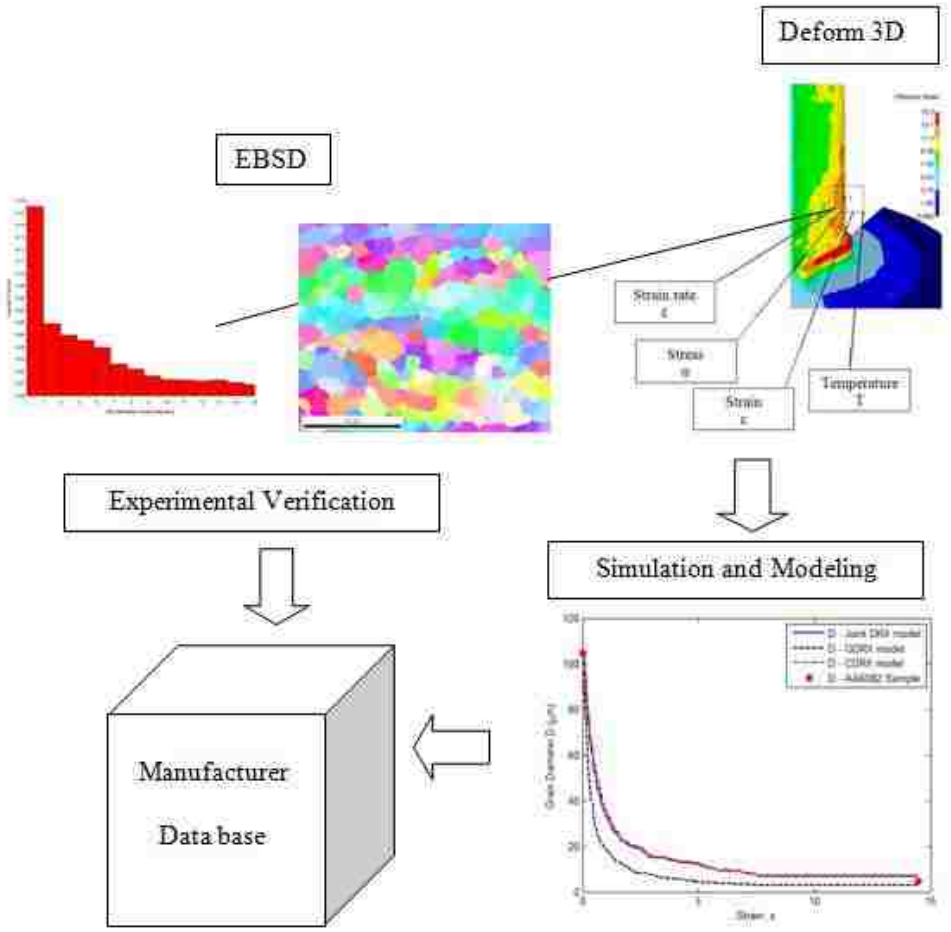

Figure 37. Illustration of how the manufacturer data can be built.

2.10 *Conclusions*

In this work, hot extrusion of AA 6082 had been investigated in the manner of the evolution of microstructure and the following conclusions were drawn:

- Light optical microscopy analysis was performed for hot extruded AA 6082 part as qualitative analysis.
- Electron back scatter diffraction (EBSD) for hot extruded AA 6082 part was performed as quantitative analysis.

- The average grain diameters were obtained for AA 6082 extruded parts with different ram speeds (0.25 ,0.5, 2, 5 mm/sec) as well as the fraction of the low angle grain boundary (LAGB).
- Four different simulation processes by using finite element package DEFORM^{TM} -3D were done to simulate the hot extrusion process for AA6082.
- State variables from the simulation were linked to three different models Joint DRX, CDRX, GDRX to predicts the average grain diameter and the fraction of LAGB and HAGB.
- The Joint DRX has been verified and showed a good a agreement to the experimental work.
- The GDRX model's predictions is the best model to predict the average grain size.
- The Joint DRX model's predictions is the best model for the fraction of LAGB.

3 Chapter 3: Microstructure Evolution of Asymmetrically Rolled AA-5182

Based on a paper presented in ASME District A 2011 Student Professional Development Conference, Temple University, Philadelphia, PA

3.1 *Introduction*

The formability of aluminum alloy can be increased by the sever plastic deformation processes such as equal channel angle pressing (ECAP), high-pressure torsion (HPT), twist extrusion (TE), multidirectional forging (MDF), accumulative roll bonding (ABR), cyclic extrusion and compression (CEC) and asymmetric rolling (ASR)[20]. Due to modification of material microstructure, the ASR process where the linear speeds at the surfaces of the upper and lower roll differ in order to impose shear on the workpiece, has been shown to be a promising, economical approach to altering the rolled microstructure of aluminum alloy sheet in such a way that it may improve material formability. Also, ASR can be achieved by changing friction between the workpiece and upper or/and lower working mill. The purpose of the ASR process is to produce intense shear deformation throughout the entire sheet thickness, as opposed to superficial shear deformation imposed by conventional rolling. The application of ASR may lead to a small grain size below 2μm.

Many studies have focused on investigating the effect of asymmetric rolling conditions on microstructure evolution [20-26]. Most of the studies are focused on the shear texture components generated by ASR, and the effect of shear texture on formability in aluminum sheets [27-35].

The ASR processing of high-purity aluminum was investigated by Cui et.al [23]. ASR was achieved until 90% reduction different asymmetry ratios where the ratio if the

upper mill roll velocity to the lower mill roll velocity differs from 1 and 4. The authors[23] claimed that the grain evolution is a result of the intense shear deformation and the compression which lead to development of sub boundaries to high angle boundaries within the deformed grains [23] . ASR followed by annealing was performed by Jin and Lloyed [26, 36] in order to produce very fine grain sizes as small as 1μm in AA5754 and in material annealed at 250 °C. Moreover, the tensile response of this fine-grained material has been compared with that of other fine grained alloys produced by alternative methods. Also, they demonstrated that it is possible to achieve a good combination of strength and ductility by producing a duplex grain structure after asymmetrical rolling followed by annealing in AA5754 [37]. Recently, Simoes et al. [38] studied ASR of 1050-O aluminum alloy sheets followed by annealing. The authors evaluated the effect of the rolling parameters on the development of shear texture components for improving formability, and grain refinement for optimization of the mechanical properties. Roumina and Sinclair [39]emphasized that deformation geometry and the variation of the reduction per pass, will affect the shear strain gradients throughout the thickness significantly at a given level of asymmetry. Also, more uniform shear strains through thickness will be affected by the large reductions per pass. However, small reductions per pass leads to lower overall shear strain magnitudes [39]. In addition, the role of the friction in the upper and lower surfaces and its effects in the texture was studied [30, 39]. Wronski and his collaborators concluded that the temperature and the degree of asymmetry affects the texture development and its hetroginity throughout the thickness of the sheet [35]

In the present work, an asymmetrically rolled AA 5182 microstructure evolution was investigated using the Light optical Microscopy (LOM). However, the fine structure was not obtained and the reasons for that will be discussed in the next sections.

3.2 *Asymmetric Rolling Experiment*

A four-pass ASR test on an AA5182-O (Al-Mg alloy, annealed) sample was carried out on the laboratory at the University of Aveiro. Each roll was driven by a separate motor, so that the roll speeds can be independently controlled by software. A schematic of the set-up is shown in Fig.38. The top and bottom rolls have the same diameter of 180 mm. The top and bottom roll speeds are 15 and 11 rpm, respectively, in the directions indicated in Fig.37, giving a relative speed ratio of 1.36. The initial, nominal dimensions of the sample were 60mm × 20mm × 8mm (rolling direction -RD × transverse rolling direction-TD × normal to rolling direction-ND). To prevent the sample from bending up or down, top and bottom guides were placed at the exit from the rolling gap.

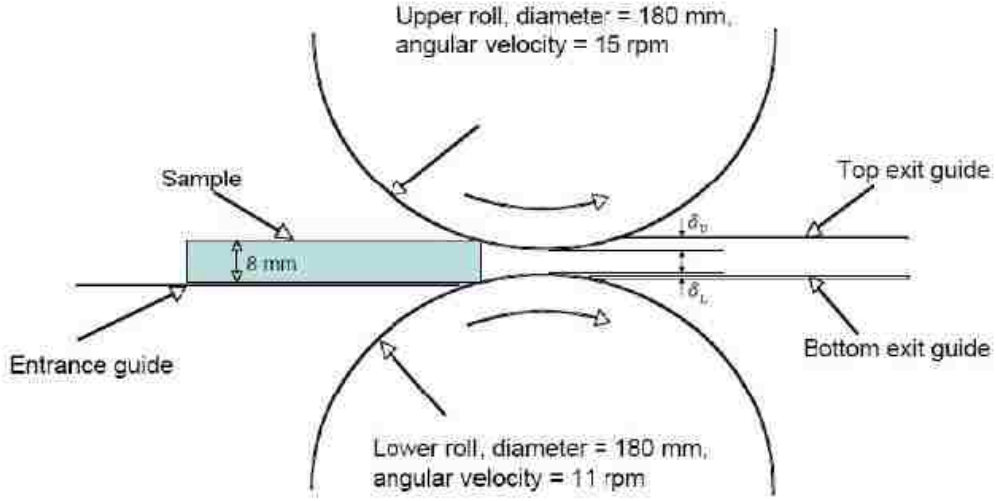

Figure 38. Schematic set-up of asymmetric rolling experiment.

For the first two passes, the sample passed through the mill in the same direction. After the second pass, the sample was rotated 180º about ND to effectively reverse the rolling direction for the last two passes. A reduction of approximately 25% was imposed for each pass, and the actual reduction was determined from measurements after each pass. The actual, measured, reduction ratios per pass and cumulative reduction ratios are listed in Table 9, where hp is the measured sample thickness for given pass .

Table 10. Measured reduction ratios for each rolling pass.

Pass	Reduction per pass (1− hp/hp−1)*100	Total reduction (1 − hp/h0)*100
1	20 %	20 %
2	25 %	39 %
3	21 %	53 %
4	28 %	66 %

3.3 *Experimental procedures*

The microstructure response to the ASR process conditions for the AA5182-O was analyzed using metallographic techniques. The initial sample microstructure and the microstructure after the first and fourth passes were analyzed at three locations in each sample - near the top face where contact with the upper roll took place, near the mid plane, and near the bottom face where contact with the lower roll took place.

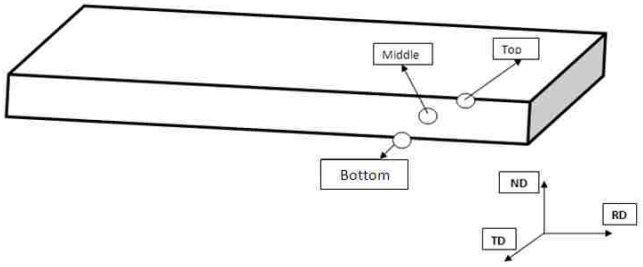

Figure 39. The specific locations of metallographic sample locations with marked rolling direction.

The specimens for analysis were cut from the sample using a Unitom-2 abrasive cut-off Struers aluminum oxide wheel and an Isomet low speed Buehler saw with a diamond wheel. The specimens were then ground with progressively finer silicon carbide papers with ANSI (CAMI) US 800 as the finest and water used as coolant. The specimens were then polished with diamond and finally silicon dioxide. Next, the samples were etched using 3% tetrafluoroboric acid (Barker's, 48%) in distilled water with a voltage of 30 V for 60-90 sec, depending on the thickness of the sample, with the most highly deformed specimen needing less time for etching due to an increased stored energy.

3.4 *Results*

The microstructures of the rolled specimens are shown in Figs. 40-42. The grain sizes were measured by using ASTM E112 specifically intercept method. It varies within the samples and much more between the samples representing different stages of the ASR process. The initial, as received, sample is shown in Fig.40, the grain size is observed to be varying from about 47 μm for the top of the sample to about 56 μm in the middle and about 58 μm near the bottom. The microstructure after one pass is shown in Fig.41, the grain size did not change significantly due to the low reduction. The grain sizes are similar to those in the initial material, but the grains are elongated along RD as

shown in Fig. 41. However, by the end of the fourth pass, the grain size has been significantly reduced as can be seen in Figs. 42. The grain size varies from about 10 μm near the top and bottom of the sample to about 13 μm in the middle. This indicates that the shearing by the ASR process used in this work is not as strong near the center as near the rolls, and thus, the deformation induced grain refinement is less near the mid-plane. These microstructures are very similar to microstructures observed in conventional rolling, where the high friction at the workpiece/ working roll interfaces induces a larger shear deformation near the rolls in addition to the plane strain compression experienced throughout the bulk of the material.

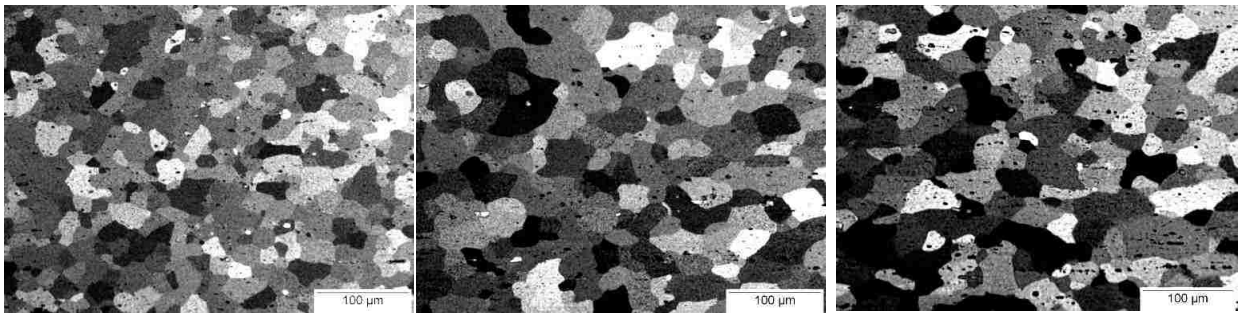

(a) (b) (c

Figure 40. The longitudinal sections of the samples of the as received (initial) material, (a) top of the sample, (b) middle of the sample, (c) bottom of the sample

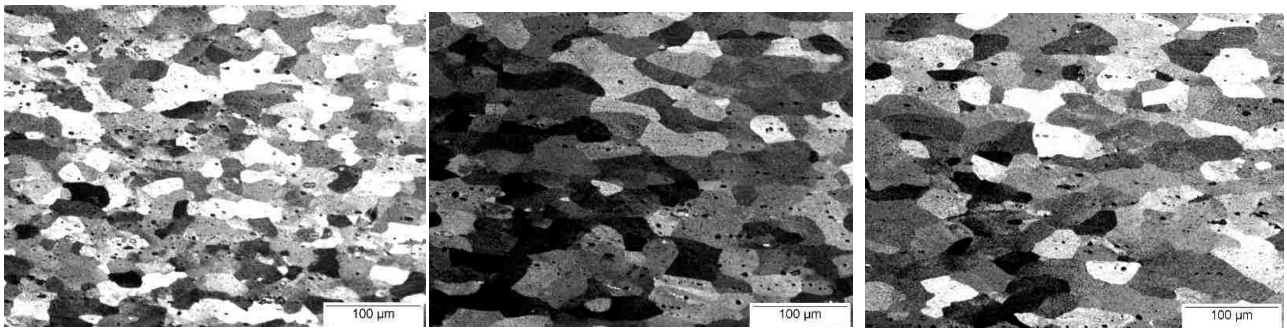

(a) (b) (c)

Figure 41.The longitudinal sections of the samples of the material after one pass (20% total reduction) , (a) top of the sample, (b) middle of the sample, (c) bottom of the sample.

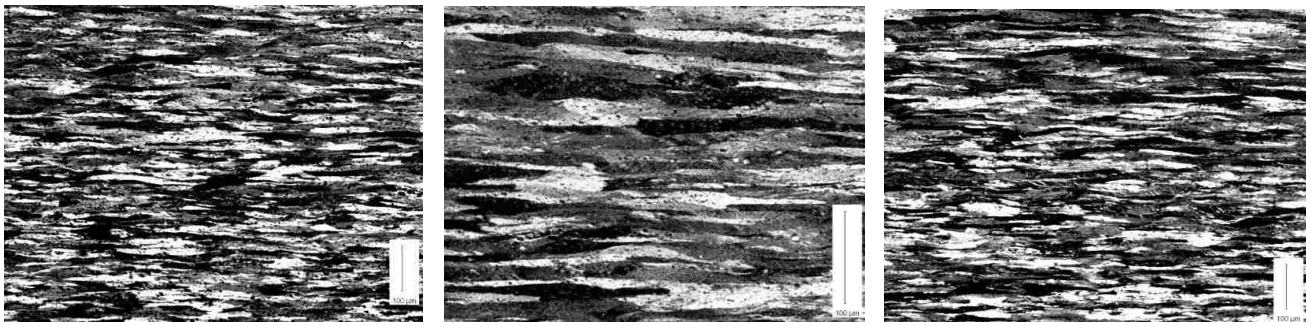

(a) (b) (c)

Figure 42. The longitudinal sections of the samples of the material after the fourth pass (66 % total reduction), (a) top of the sample, (b) middle of the sample, (c) bottom of the sample.

3.5 *Discussion*

It is well known that in the conventional rolling, the shear stress on the surface of the produced sheet will result in higher local strain and therefore produce a smaller grain size in comparison to the grain size in the middle of the sheet thickness due to the high strain rate near the surfaces. In the present work, it was expected that the differences in the diameters of the roll or the different speeds of the working rolls will be the main factor to produce the high shear stress and compression throughout the whole material thickness and subsequently a fine grain microstructure [24].

Several conditions are needed to achieve the fine grain microstructure such as high thickness reduction per pass (1− hp/hp−1)*100 which should be around 40% to 50 %. and alternating the direction of the rolling [28]. In addition the $\frac{L_P}{d}$ parameter ,where L_P is the projected length of a contacted arc between roll and sheet and d is the mean thickness of the sheet in the deformation zone Fig. 43 , should be close between 0.1 to .15 of the thickness reduction per pass to provide microstructure with finer grains [29].

$$\frac{2\,L_p}{h_o+h_f} \cong (0.1\sim0.15) * (1-\frac{h_p}{h_{p-1}}) \qquad (3\text{-}1)$$

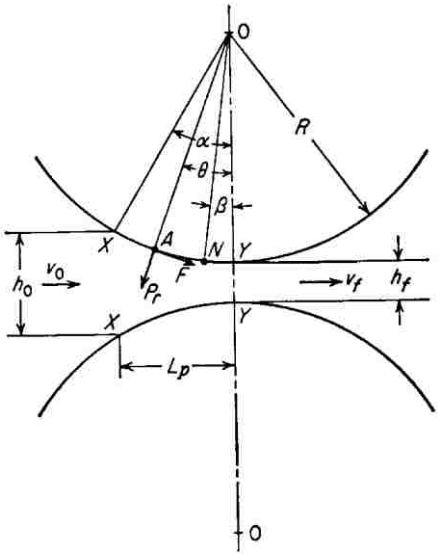

Figure 43. Schematic of the rolling process geometry [9].

In the present work the reduction per pass (20 % -28 %) was not sufficient to produce a fine grain structure as expected. Moreover, alternating the sample after each pass is needed to assure a uniform distribution of the fine grains through the thickness. Furthermore, the requirement of the rolling temperature below 150° C (423° K) of ASR is important to provide a stable fine grain [23].

The shape factor of the deformation zone geometry Δ which is defined as the ratio of the mean thickness to the projected length of the arc of contact L_P. Δ is a good indicator of a redundant work, frictional work and forming force [40].

For achieving a more uniform shear strain profile throughout the thickness, the shape factor $\Delta = \frac{h_o + h_f}{2L_p}$ should be small – less than 0.75 which means a high thickness reduction per pass [41]. Conversely, at a large Δ more strong shear strain profile will be observed [39]. When the high thickness reduction is achieved some considerations have to be taken to avoid the rolling defects such as split ends also known as alligatoring and central burst[41].

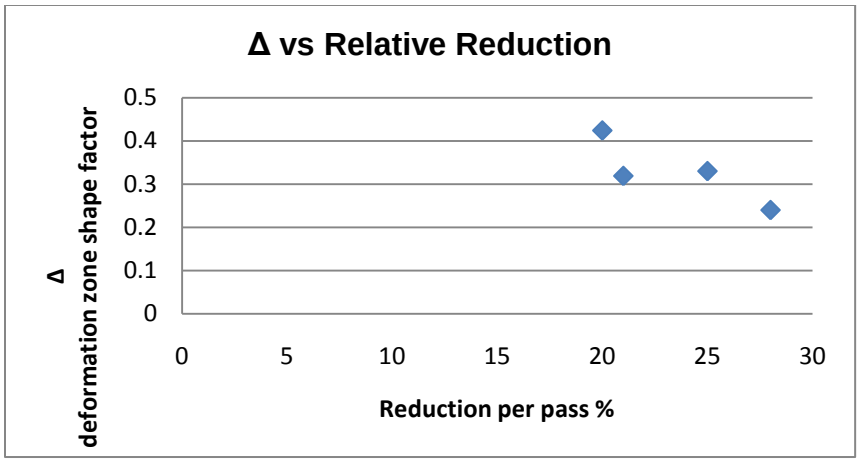

Figure 44. The deformation zone shape factor and the relative reduction for the AA5183 asymmatrically rolled.

The safe zone can be as high as 50% reduction with Δ less than 0.75 as shown in s Fig.45. The safe zone is applied for conventional rolling but it is a good indication for the asymmetrical rolling as shown in Fig.44 which indicated that they were in the safe zone . However, it has to be kept in mind that the proposed calculations may not be directly transferred to asymmetric rolling conditions.

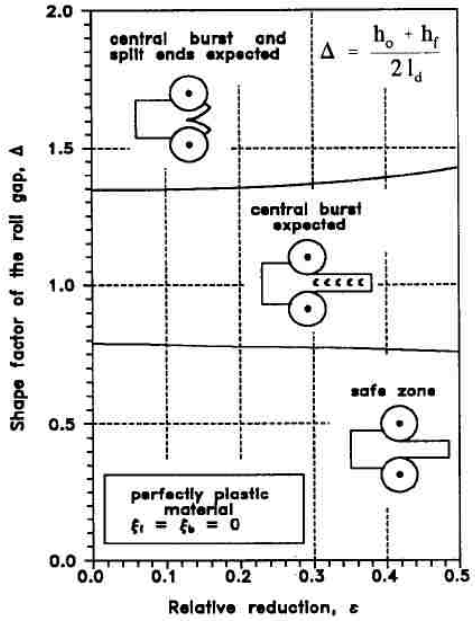

Figure 45. Influence of the roll gap shape factor on central burst and split ends defects during conventional rolling [41]

3.6 *Conclusions*

In this work, an asymmetrical rolling for AA5182 had been investigated in the manner of the evolution of microstructure and the following conclusions were drawn:

- Aluminum alloy sheet- AA5182- was asymmetrically rolled.
- Light optical microscopy analysis was performed to characterize the microstructure.
- The fine grain structure was not obtained across the entire sheet thickness.
- In order to achieve the fine grain structure many conditions should be optimized during the process. Among those condition are Δ parameter, temperature, maximum reduction per pass to ensure a uniform fine grain structure throughout the whole thickness. Meeting those conditions should allow us to obtain improved sheet formability.

4 General Summary

The presented case studies show different techniques used to predict final product microstructure. In both case, in rolling and extrusion, combination of material characterization and numerical process simulation allowed very satisfactory results for selected Aluminum alloys. The microstructure characterizations were done using Light Optical Microscopy (LOM), Electron Backscattered Diffraction (EBSD). The state variables during deformation were predicted using finite element method package DEFORM™ -3D, which were used successfully in the proposed microstructure model.

References

[1] Anonymous *ASM Specialty Handbook: Aluminum and Aluminum Alloys.* ASM International, 1993.

[2] J. W. Bray, *Aluminum Mill and Engineered Wrought Products.* ASM International, 1990.

[3] Pawel Kazanowski, *Forming of aluminum alloys* ASM International, 2006.

[4] Frank F. Kraft and Jay S. Gunasekera, *Conventional hot extrusion, metalworking: Bulk forming* ASM International, 2005.

[5] Taylan Altan, Soo-lk Oh and Harold L. Gegel, *Metal Forming: Fundamentals and Applications.* 1983.

[6] Wojciech Z. Misiolek and Richard M. Kelly, *Extrusion of aluminum alloys ,metalworking: Bulk forming* . ASM Handbook 2005.

[7] M. Bauser, G. Sauer and K. Siegert, Eds., *Extrusion.* Materials Park, Ohio: ASM International, 2006.

[8] W. Misiolek and J. Zasadzinski, "Estimation of the extrudability of metals by means of a special test die," *Archiwum Hutnictwa,* vol. 30, pp. 509-522, 1985.

[9] G. E. Dieter, *Mechanical Metallurgy.* McGraw-Hill, 1986.

[10] Mikell P. Groover, *Fundamentals of Modern Manufacturing: Materials, Processes, and Systems.* John Wiley & Sons Inc., 2006.

[11] Z. Peng and T. Sheppard, "Individual influence of forming parameters on surface recrystallization during aluminium extrusion," *Modelling and Simulation in Materials Science and Engineering,* vol. 12, pp. 43-57, 2004.

[12] F. J. Humphreys, "A unified theory of recovery, recrystallization and grain growth, based on the stability and growth of cellular microstructures--II. The effect of second-phase particles," *Acta Materialia,* vol. 45, pp. 5031-5039; 5031, Dec, 1997.

[13] F. J. Humphreys, "A unified theory of recovery, recrystallization and grain growth, based on the stability and growth of cellular microstructures--I. The basic model," *Acta Materialia,* vol. 45, pp. 4231-4240; 4231, Oct, 1997.

[14] F. J. Humphreys, "Inhomogeneous deformation of some aluminum alloys at elevated temperature," in *Strength of Metals and Alloys, Proceedings of the 6th International Conference,* Melbourne; Australia, 1982, pp. 625-630.

[15] F. J. Humphreys and M. Hatherly, *Recrystallization and Related Annealing Phenomena.* Oxford: Elsevier Ltd., 2004.

[16] L. De Pari Jr, "Direct Extrusion Process Analysis with Proposed Numerical Modeling Improvements - Product Quality, Process Parameters, and Microstructure Prediction," pp. 158, 2009.

[17] R. D. Doherty, D. A. Hughes, F. J. Humphreys, J. J. Jonas, D. J. Jensen, M. E. Kassner, W. E. King, T. R. McNelley, H. J. McQueen and A. D. Rollett, "Current issues in recrystallization: a review," *Materials Science and Engineering A,* vol. 238, pp. 219-274; 219, Nov 15, 1997.

[18] L. De Pari Jr and W. Z. Misiolek, "Theoretical predictions and experimental verification of surface grain structure evolution for AA6061 during hot rolling," *Acta Materialia,* vol. 56, pp. 6174-6185, 2008.

[19] William H. Van Geertruyden, "The origin of surface recrystallization in extrusion of 6xxx aluminum alloys," pp. 173, 2004.

[20] J. Jiang, Y. Ding, F. Zuo and A. Shan, "Mechanical properties and microstructures of ultrafine-grained pure aluminum by asymmetric rolling," *Scripta Materialia,* vol. 60, pp. 905-908, 2009.

[21] P. J. Apps, C. P. Heason and P. B. Prangnell, "Ultrafine-grain structures produced by severe deformation processing," in Zurich-Ueticon, Switzerland, 2004, pp. 423-428.

[22] Y. Chen, A. Shan, J. Jiang and Y. Ding, "Characterizing the shear deformation during asymmetric rolling," in Stafa-Zuerich, CH-8712, Switzerland, 2008, pp. 327-332.

[23] Q. Cui and K. Ohori, "Grain refinement of high purity aluminium by asymmetric rolling," in UK, 2000, pp. 1095-101.

[24] Q. Cui and K. Ohori, "Grain refinement of a 6061 aluminum alloy by asymmetric warm-rolling," *Keikinzoku/Journal of Japan Institute of Light Metals,* vol. 52, pp. 185-189, 2002.

[25] S. Fare, M. Vedani and G. Angella, "Features on grain-structure evolution during asymmetric rolling of aluminium alloys," in *International Conference Recent Developments in the Processing and Applications of Structural Metals and Alloys, June 22, 2008 - June 25,* 2009, pp. 77-85.

[26] H. Jin and D. Lloyd, "The tensile response of a fine-grained AA5754 alloy produced by asymmetric rolling and annealing," *Metallurgical and Materials Transactions A,* vol. 35, pp. 997-1006, 2004.

[27] S. Kang, B. Min, H. Kim, D. S. Wilkinson and J. Kang, "Effect of asymmetric rolling on the texture and mechanical properties of AA6111-aluminum sheet," *Metallurgical and Materials Transactions A: Physical Metallurgy and Materials Science*, vol. 36, pp. 3141-3149, 2005.

[28] S. Kim, J. Ryu, K. Kim and D. N. Lee, "The evolution of shear deformation texture and grain refinement in asymmetrically rolled aluminum sheets," *Materials Science Research International*, vol. 8, pp. 20-25, 2002.

[29] J. K. Lee and D. N. Lee, "Shear texture development and grain refinement in asymmetrically rolled aluminum alloy sheets by varied reduction per pass," in 2002, pp. 1419-1424.

[30] J. Lee and D. N. Lee, "Texture control and grain refinement of AA1050 Al alloy sheets by asymmetric rolling," *International Journal of Mechanical Sciences*, vol. 50, pp. 869-887, 2008.

[31] T. Shimamura, T. Sakai, H. Utsunomiya and S. Kaneko, "Texture and microstructure control of al-mg-si alloy sheet by differential speed rolling," in Stafa-Zuerich, CH-8712, Switzerland, 2007, pp. 1443-1447.

[32] J. Sidor, R. Petrov and L. A. I. Kestens, "Improved plastic anisotropy in asymmetrically rolled 6xxx alloy," in *3rd International Conference on Texture and Anisotropy of Polycrystals, ITAP-3, September 23, 2009 - September 25*, 2010, pp. 165-170.

[33] J. Sidor, L. Zhuang, M. Van Der Winden and L. Kestens, "Effect of asymmetric rolling on texture and anisotropy of AA6016 alloy for automotive applications," in Warrendale, PA 15086, United States, 2008, pp. 113-118.

[34] J. Sidor, R. Petrov, A. Miroux and L. Kestens, "Texture modification in asymmetrically rolled aluminum sheets," in Westerville, OH 43082, United States, 2008, pp. 547-554.

[35] S. Wronski, B. Ghilianu, T. Chauveau and B. Bacroix, "Analysis of textures heterogeneity in cold and warm asymmetrically rolled aluminium," 2010.

[36] H. Jin and D. J. Lloyd, "The different effects of asymmetric rolling and surface friction on formation of shear texture in aluminium alloy AA5754," *Materials Science and Technology*, vol. 26, pp. 754-760, 2010.

[37] H. Jin and D. J. Lloyd, "Effect of a duplex grain size on the tensile ductility of an ultra-fine grained Al–Mg alloy, AA5754, produced by asymmetric rolling and annealing," *Scr. Mater.*, vol. 50, pp. 1319-1323, 5, 2004.

[38] F. J. P. Simoes, R. J. A. de Sousa, J. J. A. Gracio, F. Barlat and J. W. Yoon, "Mechanical behavior of an asymmetrically rolled and annealed 1050-O sheet," *Int. J. Mech. Sci.,* vol. 50, pp. 1372-1380, Sep, 2008.

[39] R. Roumina and C. W. Sinclair, "Deformation geometry and through-thickness strain gradients in asymmetric rolling," *Metall Mat Trans A Phys Metall Mat Sci,* vol. 39, pp. 2495-2503, 2008.

[40] William F. Hosford, Robert Caddell,
Metal Forming: Mechanics and Metallurgy. Cambridge University Press, 2011.

[41] S. Turczyn, "Effect of the roll-gap shape factor on internal defects in rolling," *J. Mater. Process. Technol.,* vol. 60, pp. 275-282, 1996.

VITA

Nabeel Alharthi was born in Taif, Saudi Arabia. He is the son of Hussain Alharthi and Norah Alharthi. In 1996, he graduated from the high school and he moved to Jeddah to study mechanical engineering in King Abdulaziz University (KAU). In 2001, he graduated from KAU and he started his job in Saudi Arabian Monetary Agency in Riyadh as a researcher for one year. Then, he joined Saline Water Conversion Corporation in Jubail as a mechanical engineer for one year. In 2003, he moved back to Jeddah to work for Saudi Arabian Airlines for four years as a material specialist. In 2005, he went back to academic life to pursue Executive Master of Business Administration degree from King Abdulaziz University on a part time basis. While he was studying there he got a job in King Saud University at Riyadh and a scholarship to purse the Master of Science degree and Doctor of Philosophy degrees. In 2008, he joined Lehigh University, Bethlehem, PA, US. He is married and he has two children, son and daughter. Among his many hobbies are soccer and various outdoor activities.